

## Spectroscopic Follow-up of Young High- $\alpha$ Dwarf Star Candidates: Still Likely Genuinely Young

YUXI(LUCY) LU ,<sup>1,2</sup> CATHERINE MANEA ,<sup>3</sup> MARYUM SAYEED ,<sup>4</sup> STEPHANIE T. DOUGLAS ,<sup>5</sup> MADELEINE MCKENZIE ,<sup>6</sup> DOMINICK ROWAN ,<sup>1,2,7</sup> ILYA ILYIN ,<sup>8</sup> ADAM WHEELER ,<sup>9</sup> SVEN BUDER ,<sup>10,11</sup> LOUIS AMARD ,<sup>12</sup> MARC H. PINSONNEAULT ,<sup>1,2</sup> AND JENNIFER A. JOHNSON<sup>1,2</sup>

<sup>1</sup>Department of Astronomy, The Ohio State University, Columbus, 140 W 18th Ave, OH 43210, USA

<sup>2</sup>Center for Cosmology and Astroparticle Physics (CCAPP), The Ohio State University, 191 W. Woodruff Ave., Columbus, OH 43210, USA

<sup>3</sup>Department of Physics & Astronomy, University of Utah, Salt Lake City, UT 84112, USA

<sup>4</sup>Department of Astronomy, Columbia University, 550 West 120<sup>th</sup> Street, New York, NY, USA

<sup>5</sup>Lafayette College, 730 High St, Easton, PA 18042, USA

<sup>6</sup>Carnegie Observatories, 813 Santa Barbara St, Pasadena, CA, 91101, USA

<sup>7</sup>Department of Astronomy, University of California Berkeley, Berkeley, CA 94720, USA

<sup>8</sup>Leibniz-Institute for Astrophysics Potsdam (AIP), An der Sternwarte 16, D-14482, Potsdam, Germany

<sup>9</sup>Center for Computational Astrophysics, Flatiron Institute, 162 5th Avenue, New York, NY 10010, USA

<sup>10</sup>Research School of Astronomy & Astrophysics, Australian National University, Canberra ACT 2611, Australia

<sup>11</sup>Center of Excellence for Astrophysics in Three Dimensions (ASTRO-3D), Australia

<sup>12</sup>Departemnt of Astronomy, University of Geneva, Chemin Pegasi 51, CH-1290 Versoix, Switzerland

## ABSTRACT

The question of whether genuinely young high- $\alpha$  stars exist has been discussed for over a decade since their discovery from asteroseismology of giant stars as it is challenging to break the degeneracy between the binary interaction and the genuinely young scenarios. Young high- $\alpha$  stars are hard to explain with traditional chemical evolution model as the high- $\alpha$  disk is typically associated with the early epoch of star formation in the Milky Way. Combined with recent advances of gyrochronology, and that  $^7\text{Li}$  can serve as an unambiguous indicator for identifying merger products in dwarfs thanks to its low burning temperature, we identified young high- $\alpha$  dwarf candidate stars through their fast rotation in a previous study. In this paper, we performed high-resolution spectroscopic follow-up of these candidates using Potsdam Echelle Polarimetric and Spectroscopic Instrument (PEPSI), and confirm 3 additional stars that are most likely genuinely young. Together with the star from the earlier paper, we find three out of four of them center around  $[\text{Fe}/\text{H}] = -0.5$  dex, are  $\sim 5$  Gyr old, and have a similar amount of elevated Li ( $\sim 0.5$  dex) and Al ( $\sim 0.1$  dex) compared to stars with matching  $\log g$ ,  $T_{\text{eff}}$ , Mg, and Fe within observational uncertainties, hinting at their common formation pathway.

**Keywords:** Stellar ages (1581) — Stellar rotation (1629) — Galaxy abundances (574) — Galaxy formation (595) — Galaxy dynamics (591) — Galaxy chemical evolution (580)

## 1. INTRODUCTION

The discovery of stars with enhanced  $\alpha$ -element abundances yet unexpectedly young ages presents a significant challenge to conventional models of Galactic chemical evolution (Chiappini et al. 2015; Martig et al. 2015; Silva Aguirre et al. 2018; Claytor et al. 2020; Das et al.

2020; Zinn et al. 2022; Grisoni et al. 2024; Lu et al. 2025). These so-called “young high- $\alpha$  stars” are particularly puzzling because  $[\alpha/\text{Fe}]$  is positively correlated with the ratio of enrichment from Type II Supernova (produced by exploding massive stars) to enrichment from Type Ia Supernova (produced by white dwarf mergers or accretions). Stars with enhanced  $[\alpha/\text{Fe}]$  are typically associated with rapid early star formation in the Milky Way, where star formation efficiency is high (e.g., Connroy et al. 2022), implying ages greater than  $\sim 8$  Gyr. Yet, mounting evidence mostly from asteroseismology (e.g.,

Corresponding author: Yuxi(Lucy) Lu  
 lucylulu12311@gmail.com

Chiappini et al. 2015; Martig et al. 2015; Silva Aguirre et al. 2018; Zinn et al. 2022; Grisoni et al. 2024; Jofré et al. 2023), and from stellar rotation (Claytor et al. 2020; Lu et al. 2025) has revealed a small but robust population of  $\alpha$ -enhanced stars that appear significantly younger. The creation of these young high- $\alpha$  stars could be possible but typically requires rapid local enrichment without phase mixing the star-forming gas (e.g., Johnson et al. 2021; Garver et al. 2023).

One major difficulty in interpreting these stars is disentangling true youth from the effects of binary evolution. Asteroseismology measures the current mass of the star, which is related to age under the assumption that the star has experienced no significant interactions during its lifetime. As a result, the asteroseismic candidates are more precisely defined as massive  $\alpha$ -rich stars, which are young for a normal stellar evolution history. However, mass transfer, mergers, or tidal spin-up in close binaries can all conspire to obscure a star's true age, either by increasing its mass or by altering its surface properties (e.g., Tayar et al. 2015; Yong et al. 2016; Jofré et al. 2016; Hekker & Johnson 2019; Zhang et al. 2021; Jofré et al. 2023; Cerqui et al. 2023; Grisoni et al. 2024; Izzard et al. 2018). For red giants, stellar mergers are difficult to distinguish from genuinely young stars. Merger products spin down quickly as stars expand, so they need not be rapid rotators. Most chemical species are not impacted if both stars are on, or close to, the main sequence.

Lithium is an interesting exception to this general guideline. Li provides direct evidence for distinguishing between merger and genuinely young scenarios: it is easily destroyed during main-sequence star mergers (e.g., Ryan et al. 2001; Pinsonneault et al. 2002; Ryan et al. 2002), as the thin convective envelope and limited Li reservoir means Li can be quickly depleted by heating associated with mass transfers. The relatively shallow convection zones of dwarf stars mean that Li is less diluted compared to in evolved stars, making it easier to detect.

By leveraging gyrochronology as an age indicator for dwarf stars (Barnes 2003), Lu et al. (2025) discovered one likely true young high- $\alpha$  star and a list of similar candidates using Kepler (Borucki et al. 2010) and K2 (Howell et al. 2014) for rotation period measurements, and APOGEE (Majewski et al. 2017) and GALAH (De Silva et al. 2015) for abundances. To exclude binary interactions, not only do we need Li detections, but close-in binaries also need to be excluded, as they can tidally spin-up a star without any mass transfer (e.g., Meibom & Mathieu 2005; Lurie et al. 2017; Simonian et al. 2019). Unfortunately, most of these candidates identified in

Lu et al. (2025) only have data from GALAH, which lacks multi-epoch radial velocity (RV) needed to exclude close-in binaries, or are only observed in APOGEE, which lacks Li measurements.

In this paper, we present new high-resolution spectroscopic follow-up of some of the young high- $\alpha$  dwarf star candidates from Lu et al. (2025) to investigate their chemical abundances, binary information, kinematics, and Li content in detail. Our goal is to further test whether any high- $\alpha$  dwarf stars are genuinely young and their possible formation pathways. The target selection is described in Section 2.1. Analysis procedure including reduction (Section 2.2), RV measurements and corrections (Section 2.3), abundance measurement (Section 2.4), period measurement (Section 2.5), initial candidate exclusion (Section 2.6), binary analysis (Section 2.7), and comparisons with doppelgänger stars with similar global properties in spectra Signal-to-Noise (SNR), Mg or  $\alpha$ , Fe,  $\log g$ , and  $T_{\text{eff}}$  (Section 2.8) are shown in Section 2. Using these results, we analyze each of the three genuinely young high- $\alpha$  stars in Section 3.1. In Section 3.2, we examine the chemical patterns of all four genuinely young high- $\alpha$ . We also highlight one possible merger product in Section 3.3. We discuss their possible formation pathways in Section 3.4. Finally, we summarize our findings and discuss future directions in Section 4.

## 2. DATA & SELECTION

### 2.1. Target & Filter Selections

We use the Potsdam Echelle Polarimetric and Spectroscopic Instrument (PEPSI, Strassmeier et al. 2015), mounted on the the 11.8 m Large Binocular Telescope (LBT; e.g., Hill et al. 2012) in Arizona to perform spectroscopic follow-up. We choose its lowest spectral resolution of  $R \sim 50,000$  to minimize the exposure time.

We selected 5 stars from the GALAH-K2 young high- $\alpha$  candidate sample in Table 1 of Lu et al. (2025) for radial velocity follow-up and 11 stars from the APOGEE-Kepler/K2 young high- $\alpha$  candidate sample to obtain Li abundances. The stars in Lu et al. (2025) Table 1 are high in  $[\alpha/\text{Fe}]$  from APOGEE or GALAH. The definitions for high- $\alpha$  in Lu et al. (2025) are  $[\alpha/\text{Fe}] > -0.6[\text{Fe}/\text{H}] + 0.20$  for APOGEE, and  $[\alpha/\text{Fe}] > -0.3[\text{Fe}/\text{H}] + 0.19$  for GALAH. Young stars rotate more rapidly than old ones, so we select stars with rotation below  $<\sim 35$  days, or  $<\sim 8$  Gyr, which is the typical age of the high- $\alpha$  disk. However, synchronized binaries exist with period less than 15 days, so our best candidates have periods between 15 and 35 days. Besides all the requirements mentioned above, all the APOGEE stars are selected to have more than two RV measurements

agreeing within 1 km/s to vet for close-by stellar binaries that can spin-up the stars, and the GALAH stars are also selected to have Li measurements from [Wang et al. \(2024\)](#), since we want to use Li as a mass-transfer diagnostic. Finally, we can use  $vsini$  as an alternative measurement of rotation and synchronized binaries, and thus, we also remove stars with  $vsini > 10$  km/s.

For the spectroscopic follow-up, we selected relatively bright stars with Gaia  $G$ -band magnitudes  $\lesssim 14$  mag to minimize the exposure time, and were observable from the LBT for the October 2024 to December 2024 observing season. We selected cross dispersions settings CD3 (wavelength range of 480.0-544.1 nm) and CD5 (wavelength range of 627.8-741.9 nm) to capture important abundance information, including reliable  $\alpha$  element lines (Mg, Ca, Si) and the Li 6707 Å line. We want to obtain Li for stars only in APOGEE as APOGEE observes in the infrared and does not include the Li line. The Li measurements from PEPSI will also serve as an independent confirmation of Li for stars in GALAH. In the end, we were able to obtain spectra for 9 APOGEE-Kepler/K2 young high- $\alpha$  candidate stars and 4 GALAH-K2 young high- $\alpha$  candidate stars. Their IDs,  $V$  magnitudes, number of observations, representative SNR values close to the Li line calculated for the combined spectra, observation days, and exposure times are shown in Table 1.

## 2.2. PEPSI Spectra Reduction

The PEPSI 2D echelle spectra are reduced following the procedure described in [Strassmeier et al. \(2018\)](#). The standard reduction include bias over-scan detection and subtraction, scattered light surface extraction and subtraction, definition of échelle orders, weighted extraction of spectral orders, wavelength calibration, and a self-consistent continuum fit to the full 2D image of extracted orders. For each spectrum, Least-Squares Deconvolution (LSD) is also performed in CD3 using PHOENIX model spectra ([Husser et al. 2013](#)) that are close in  $T_{\text{eff}}$  and  $\log g$  to vet for spectroscopic binaries.

## 2.3. Radial Velocity Measurements & Corrections

We measure radial velocities (RVs) with iSpec ([Blanco-Cuaresma et al. 2014](#)), which uses 1D cross-correlation with the synthetic Solar template provided with the installation. We use a wavelength range of 4760 – 5500 Å to measure the RV, and the RV uncertainties are determined following [Zucker \(2003\)](#). The typical uncertainty associated with our analysis is on the order of 0.05 km/s.

## 2.4. Abundance Measurements

For stars with more than one observation, we first corrected the RV shift for the individual spectrum. The final spectrum used to obtain abundances were then obtained from co-adding the individual spectra by taking the mean.

For these stars, we are mostly interested in their  $\alpha$  (Mg, Ca, Si) and Li abundances from PEPSI to independently confirm their high  $\alpha$  and investigate their Li abundances. However, we also determine elemental abundances of other species (C, Al, Sc, Ti, V, Cr, Mn, Co, Ni, Cu, Zn, Y, Zr, Ba, Ce, Nd) to obtain a full chemical profile for each star using our higher resolution ( $R \sim 50,000$ ) spectra and validate survey abundances. To determine stellar abundances, we must first assume a set of stellar parameters ( $T_{\text{eff}}$ ,  $\log g$ , microturbulence ( $v_{\text{micro}}$ ), metallicity). We adopt  $T_{\text{eff}}$  and  $\log g$  from either APOGEE or GALAH where available due to their superior precision (MAYBE WE CAN MENTION THE TEFF AND LOGG PRECISION HERE?). We then use Brussels Automatic Code for Characterizing High accuracy Spectra (BACCHUS, [Masseron et al. 2016](#)) to determine  $v_{\text{micro}}$ , spectral broadening (which includes instrumental broadening and  $vsini$ ), and individual elemental abundances for up to 20 elements (excluding Li, which is treated separately) from the reduced and continuum normalized PEPSI spectra. BACCHUS is a spectral synthesis and fitting code designed for high-resolution spectra. It uses Turbospectrum ([Plez 2012](#)) to synthesize spectra and determines line-by-line abundances using four distinct fitting methods. We point readers to [Hayes et al. \(2022\)](#) and [Manea et al. \(2025\)](#) for a detailed description of BACCHUS and its fitting methods. We interpolate over the MARCS model atmosphere grid ([Gustafsson et al. 2008](#)) with BACCHUS for our stellar atmospheric models, and we assume one-dimensional local thermodynamic equilibrium (1D LTE) throughout our analysis. For our atomic data, we use version 5 of the *Gaia*-ESO linelist ([Heiter et al. 2021](#)) and combine molecular transition data from numerous sources: CH from [Masseron et al. 2014](#), C2, CN, OH, and MgH from T. Masseron, private communication, SiH from [Kurucz 1992](#), and TiO, FeH, and ZrO from B. Pelz, private communication. For our line selection, we begin with lines that [Heiter et al. \(2021\)](#) indicates have reliable  $\log gf$  values ( $gffflag = Y$ ) and are unblended (or only blended with lines of the same species) in the Solar and Arcturus spectrum ( $synflag = Y$ ). We then only retain lines that return consistent (within 0.1 dex) abundances across the four BACCHUS abundance determination methods. This discards lines that are saturated or otherwise poorly modeled by the synthetic spectra. Our final elemental abundances are determined

Sample	2MASS ID	Gaia DR3 ID	V mag	N Obs.	Comb. SNR	Obs. Date	Exp. Time [s]
A–K2	03413908+2359163	68164639977312384	13.9	2	103	Oct. 25, 2024	1440
...	...	...	...	...	...	Nov. 1, 2024	1440
G–K2	03435417+1719250	44497171153467008	11	7	132	Sep. 20, 2024	240
...	...	...	...	...	...	Oct. 8, 2024	160
...	...	...	...	...	...	Oct. 8, 2024	160
...	...	...	...	...	...	Oct. 23, 2024	120
...	...	...	...	...	...	Oct. 31, 2024	120
...	...	...	...	...	...	Oct. 31, 2024	120
...	...	...	...	...	...	Nov. 1, 2024	240
G–K2	01084954-0030464	2533196969884293888	13.6	3	82	Oct. 21, 2024	1200
...	...	...	...	...	...	Oct. 31, 2024	1200
...	...	...	...	...	...	Nov. 24, 2024	600
A–K	18432994+4356589	2117326900207932288	14.2	1	47	Sep. 20, 2024	1800
G–K2	01064189-0027182	2533233700444556800	13.8	5	111	Sep. 22, 2024	1320
...	...	...	...	...	...	Oct. 10, 2024	1780
...	...	...	...	...	...	Oct. 10, 2024	1780
...	...	...	...	...	...	Oct. 23, 2024	1320
...	...	...	...	...	...	Oct. 31, 2024	1320
G–K2	08280198+1913343	662897729347117312	13.0	4	85	Oct. 8, 2024	800
...	...	...	...	...	...	Oct. 8, 2024	800
...	...	...	...	...	...	Oct. 25, 2024	600
...	...	...	...	...	...	Nov. 1, 2024	600
A–K2	01231989+0031088	2534334689540935040	13.5	1	71	Oct. 25, 2024	1200
A–K2	01244193+0124528	2559177811173201920	12.9	5	92	Oct. 8, 2024	780
...	...	...	...	...	...	Oct. 8, 2024	780
...	...	...	...	...	...	Oct. 21, 2024	600
...	...	...	...	...	...	Oct. 31, 2024	600
...	...	...	...	...	...	Oct. 31, 2024	600
A–K2	04314519+2502357	150907970912262016	13.7	1	117	Sep. 20, 2024	1320
A–K2	08443258+1116500	601835320304886400	13.7	1	50	Nov. 24, 2024	1020
A–K	19101724+4944353	2132794829787857792	10.3	1	35	Sep. 19, 2024	30
A–K	19380704+4708008	2128545109969957888	12.3	1	27	Oct. 25, 2024	1200
A–K	19580796+4052023	2075066724134857344	14.3	1	35	Sep. 20, 2024	2100

**Table 1.** Sample name (G–K2: GALAH–K2; A–K2: APOGEE–K2; A–K: APOGEE–Kepler), 2MASS ID, Gaia DR3 ID, V magnitudes, number of observations, representative SNR values using wavelength range 6688–6695 Å calculated for the combined spectra, observation dates, and exposure times for the sample of observed stars. The first three stars are the genuinely young rotators (see Section 3.1), and the fourth star is the possible merger product (see Section 3.3).

by taking average abundances from all reliable lines of the same species. For elements with multiple lines, the line-to-line abundance dispersion is adopted as our uncertainty, and for elements with just one line, we assume an uncertainty of 0.1 dex. Again, this excludes Li, which we treat separately and discuss in a later paragraph. We present our line-by-line abundances in Table 2, which are reported in [X/H] form assuming solar abundances from Grevesse et al. (2007).

Figure 1 compares our abundances determined from the PEPSI spectra to those from the published catalogs of APOGEE DR17 (Abdurro’uf et al. 2022) and

GALAH DR3 (Buder et al. 2021; Wang et al. 2024). For reference, we also include our abundance determinations for a PEPSI spectrum of the Sun from Strassmeier et al. (2018) that we degraded to  $R=50,000$  with iSpec and trimmed to match the wavelength limits of the rest of our spectra. We observe non-negligible abundance offsets in some elements (Mg, Ca, Fe, Ni, Cu, Zn, Y, Zr, Ba, and Ce) between our PEPSI results and those reported by APOGEE and GALAH. These offsets are also seen in our analysis of the Solar PEPSI spectrum and can be explained by differences in the spectral data, line selections, model atmospheres, adopted microturbu-

Species	Wavelength	2MASSJ03435417	2MASSJ01064189	...	2MASSJ08280198	2MASSJ19380704	Sun
C I	5052.1			...	-0.53		0.04
C I	5380.3		-0.09	...			
C I	6587.6			...			0.09
C I	7111.5			...			
C I	7113.2		-0.24	...			0.01
[O I ]	6300.3			...		0.43	0.14
Al I	6696.0	-0.97	-0.33	...	-0.58	-0.44	0.09
Al I	6698.7			...			0.1
Mg I	6318.7	-0.66	-0.19	...		-0.13	0.24
Mg I	6319.2			...		-0.24	0.17
Mg I	6319.5			...			0.33
Si II	6347.1	-0.69	-0.13	...	-0.21		0.14
Si II	6371.4	-0.73		...	-0.36	-0.33	
Si I	6721.8	-0.88		...	-0.59		-0.01
Si I	6741.6		-0.23	...	-0.29		0.09
Ca I	5260.4	-0.97	-0.46	...	-0.85	-0.28	-0.02
Ca I	5349.5	-0.8	-0.34	...	-0.7	-0.09	0.09
Ca I	6439.1	-0.88	-0.49	...	-0.56		
Ca I	6471.7	-0.87		...	-0.63		0.1
Ca I	6499.6	-0.96	-0.45	...	-0.63	-0.36	0.12
Ca I	5261.7	-0.97	-0.4	...	-0.74	-0.26	0.14
Ca I	6455.6	-1.01	-0.48	...	-0.7		-0.01
Ca I	6456.9	-0.46	-0.1	...	-0.29		
Ca I	6493.8	-0.67	-0.44	...	-0.63	-0.56	0.06
...	...	...	...	...	...	...	...
Ba II	6496.9	-0.76		...	-0.67		0.19
La II	4804.0		1.03	...			0.21
La II	5303.5		0.86	...			
La II	6390.5		0.88	...			0.08
Ce II	4914.9	-0.01		...			
Ce II	5117.2	-0.14		...			
Ce II	5187.5			...	-0.62		0.12
Ce II	5274.2			...			-0.05
Ce II	5330.6			...			-0.18
Pr II	5259.6		0.65	...			
Pr II	5322.7			...			0.1
Nd II	4811.3		1.04	...			0.29
Nd II	4914.4		0.75	...			
Nd II	4947.0		0.59	...			0.17
Nd II	4989.9		0.94	...			0.12
Nd II	5089.8		0.59	...			
Nd II	5092.8		0.73	...	-0.46		
Nd II	5234.2		0.68	...			
Nd II	5293.2		0.74	...			
Nd II	5311.5		0.78	...			
Nd II	5319.8	-0.84		...			
Nd II	5357.0		0.83	...			
Nd II	6365.5		0.65	...			
Eu II	6645.1		-0.05	...			

**Table 2.** BACCHUS-determined line-by-line abundances (reported as [X/H], assuming solar abundances from Grevesse et al. 2007) for our PEPSI spectra. Final abundances and uncertainties are determined by taking the mean and standard deviation across all lines, respectively. The full table is available in the published version of this manuscript.

lences, and abundance determination methods between this work and those of APOGEE and GALAH (e.g., [Bedell et al. 2014](#); [Ness et al. 2015](#); [Xiang et al. 2019](#)). Upon correcting for these offsets using the solar abundance offsets, we find that [Mg, Ca, Si, and Fe/H], our primary elements of interest for this portion of the analysis, agree with survey abundances within uncertainties ( $0.03 \leq \sigma \leq 0.09$  dex). Thus, our PEPSI analysis validates the high  $[\alpha/\text{Fe}]$  abundances reported by GALAH and APOGEE for this sample. The remaining elemental abundances also typically agree with survey results within abundance uncertainties after correcting for offsets with some exceptions (V, Co, and Nd).

The Li analysis was done independently and used the GALAH Li linelist. To do so, we used `Korg`, a fast 1D LTE spectral synthesis code ([Wheeler et al. 2023](#)). We adopted the  $\log g$  and  $T_{\text{eff}}$  values from APOGEE DR17 or GALAH DR3 catalogs as inputs to `Korg` to increase efficiency. We then fit the rest of the global parameters, namely metallicity ( $[\text{M}/\text{H}]$ ), microturbulence ( $v_{\text{mic}}$ ), and rotation broadening ( $v\sin i$ ). Finally, we fit for Li while fixing the global parameters. The linelist is taken to be the same as GALAH DR3 ([Buder et al. 2021](#)), as it includes the Li lines and various iron lines around it. The Li abundance  $A(\text{Li})$  from `Korg` is calculated using  $[\text{Li}/\text{H}] + 1.05$ , that is, with the Solar Li abundance from [Asplund et al. \(2009\)](#). The bias and variances for each measurement are shown in the figure legends. Even though there exist offsets between the surveys, the variance in the abundances is relatively small (typically  $< 0.1$  dex). Again, these offsets are expected, as differences of up to  $\sim 0.1$  dex are common between surveys due to variations in instruments, reduction pipelines, wavelength coverage, and fitting methodologies (e.g., [Bedell et al. 2014](#); [Ness et al. 2015](#); [Xiang et al. 2019](#)). The best-fit model and data for the Li, Ca, and Mg lines are shown in the middle row in their respective figures (Figure 3-6). The data around the  $\text{H}\alpha$  line is also shown for 18432994+4356589, as emission is seen in the core of the line (Figure 6).

## 2.5. Rotation Period Measurements

For the young high- $\alpha$  candidate stars, we downloaded the light curves using `lightkurve` ([Lightkurve Collaboration et al. 2018](#)). The rotation periods are determined following the same procedure as in [Lu et al. \(2025\)](#). They are measured using the Lomb-Scargle Periodogram implemented in `astropy` ([Astropy Collaboration et al. 2013](#); [Price-Whelan et al. 2018](#); [Astropy Collaboration et al. 2022](#)), with an over-sampling rate around the peak to be 100. The raw light curve, periodogram, and the folded light curve on the best detected period are

shown in the top row three plots in their respective figures (Figure 3-6). For the only star with Kepler data, 18432994+4356589, we perform and show the analysis for two different sectors (Figure 6).

## 2.6. Initial rejections

For the APOGEE-Kepler/K2 sample, since the binary information is mostly known from multiple RV epochs, the purpose of the spectral follow-up would be to vet for stars with Li measurements in support that they have not gone through stellar merger or mass transfer events. For this purpose, we rejected 7 out of 9 stars without significant Li detection. However, it is worth pointing out that even solar-age stars can have a range of Li depletion factors (e.g., [Jones et al. 1999](#)), for example, the Sun has a extremely low Li measurement, even though it is only 5 Gyr old. As a result, some of these stars we rejected may still be young, but we cannot prove this with Li. However, a high abundance is a reliable indicator of youth. Out of the rejected stars, we still analyzed 18432994+4356589 in detail in Section 3.3 as an potential binary product as it is confirmed to be a high- $\alpha$  star, exhibits fast rotation and high- $\alpha$  emission, but does not have Li detection.

Figure 2 left column shows our definition of the high- $\alpha$  disk (red dashed lines), abundance measurements from public surveys (red crosses: APOGEE, blue crosses: GALAH), and PEPSI (points). We defined the line separately for GALAH and APOGEE as their  $[\text{Mg}/\text{Fe}]$ - $[\text{Fe}/\text{H}]$  plane exhibits slightly different structures. Using this criterion, we further excluded 19101724+4944353 from our APOGEE sample. Therefore, we are left with 03413908+2359163 from the APOGEE-Kepler/K2 sample. The black outlined points show the genuinely young dwarf stars that we will discuss more in detail in Section 3.1.

After the initial exclusion, we only performed detailed analysis, including the binary analysis (Section 2.7) and comparison with doppelgänger stars (Section 2.8), for 03413908+2359163, 03435417+1719250, 01084954-0030464, and 18432994+4356589. These stars are shown as the top 4 entries in Table 1.

The right column in Figure 2 shows the Kiel diagrams. The points show the stars with follow-up PEPSI observations, and the black outlined points show the truly young dwarf stars, as seen in the  $[\text{Mg}/\text{Fe}]$ - $[\text{Fe}/\text{H}]$  plots. We also plotted high- $\alpha$  stars with  $-0.6 \text{ dex} < [\text{Fe}/\text{H}] < -0.4 \text{ dex}$  in dark gray points for comparison. The fact that some of the points do not hug the left edge of the distribution of the dark gray points suggest they are likely younger than the full high- $\alpha$  population. However, for the main-sequence stars, the isochrone tracks overlap

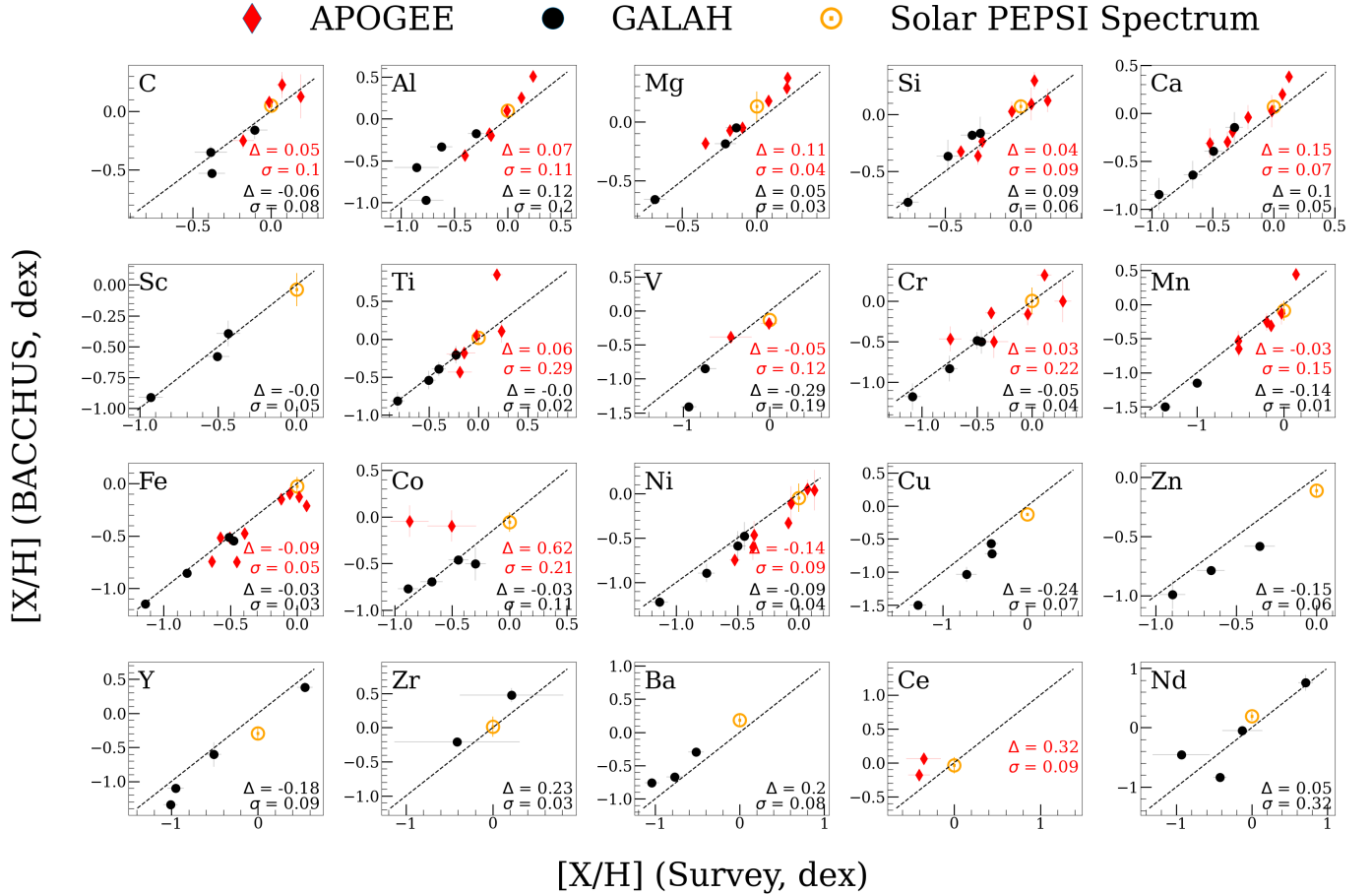


**Figure 1.** Fitting results for PEPSI using BACCHUS compared to results from APOGEE DR17 (Abdurro’uf et al. 2022) in red and GALAH DR3 (Buder et al. 2021) in black. The bias ( $\Delta$ ) and variance ( $\sigma$ ) are shown in each panel. Abundances measured from a PEPSI solar spectrum are also shown for reference to track potential abundance offsets.

heavily, and it is known that isochrone ages are not accurate for these stars, and worse, often overestimate their ages by more than 50% (Byrom & Tayar 2024). Moreover, 03413908+2359163, the one truly young dwarf star in the APOGEE-K2 sample outlined in black in the top row has a high reddening value,  $E(G_{\text{BP}} - G_{\text{RP}}) \sim 0.5$ , estimated using the 3D dustmap `bayestar2019` (Green et al. 2019), implemented in `dustmap` (Green 2018; Green et al. 2018). This high reddening value could also affect the estimations of  $T_{\text{eff}}$ ,  $\log g$ , and age for this star.

### 2.7. Binary Analysis

We use RVs and Gaia RUWE to place constraints on possible companions to each candidate, using an updated version of the Multi Observational Limits on Unseen Stellar Companions (MOLUSC; Wood et al. 2021)

tool.<sup>1</sup> MOLUSC uses rejection sampling to infer the posterior probability distribution on binary companion parameters: orbital period  $P_{\text{orb}}$ , eccentricity  $e$ , inclination  $i$ , mass ratio  $q$ , argument of periaxis  $\omega$ , pericenter phase  $\phi$ , and system RV  $v_{\text{sys}}$ . The prior is flat for  $0 \leq q \leq 1$ ,  $0 \leq \phi \leq \pi$ ,  $0 \leq \omega \leq 2\pi$ , and  $0 \leq \cos i \leq 1$ . We use a log-flat prior on  $P_{\text{orb}}$ . For  $e$ , we use a normal distribution for  $P_{\text{orb}} < 1000$  d and a uniform distribution for  $P_{\text{orb}} \geq 1000$  d. The normal distribution has the same parameterization as in Wood et al. (2021):

$$\mu_e = 0.148 \log_{10}(P_{\text{orb}}) + 0.001 \quad (1)$$

$$\sigma_e = 0.042 \log_{10}(P_{\text{orb}}) + 0.128 \quad (2)$$

We start with 50 million candidate companions sampled randomly from the prior. We calculate the predicted RV semiamplitude  $K$  for each simulated companion, and numerically solve the Kepler Equation at each

<sup>1</sup> <https://github.com/stephtdouglas/MOLUSC>, [https://github.com/stephtdouglas/lu\\_highalpha](https://github.com/stephtdouglas/lu_highalpha)

[https://github.com/stephtdouglas/lu\\_highalpha](https://github.com/stephtdouglas/lu_highalpha)

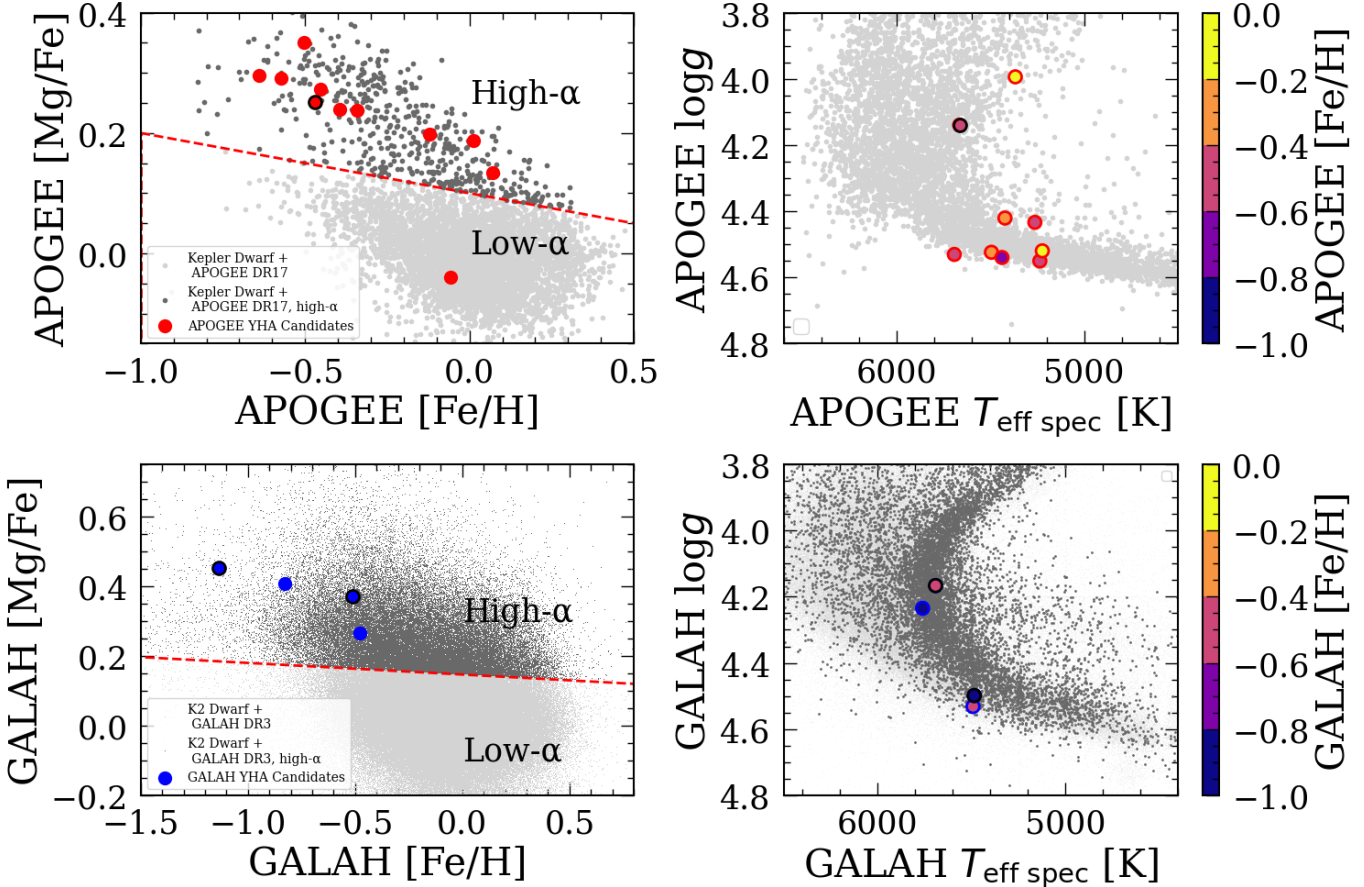


**Figure 2.** The left column shows the  $[\text{Mg}/\text{Fe}]\text{-}[\text{Fe}/\text{H}]$  plane for the APOGEE sample (top left) and GALAH sample (bottom left). The background gray points show the Kepler dwarf stars in the APOGEE field or the K2 dwarfs in the GALAH field for reference. The dark gray points show the high- $\alpha$  stars in each survey for reference. The points show the  $[\text{Mg}/\text{Fe}]$  and  $[\text{Fe}/\text{H}]$  values from APOGEE DR17 and GALAH DR3. The red dashed lines —  $[\text{Mg}/\text{Fe}] = -0.1[\text{Fe}/\text{H}] + 0.1$  for APOGEE, and  $[\text{Mg}/\text{Fe}] = -0.03[\text{Fe}/\text{H}] + 0.15$  for GALAH — show our separation for the high- and low- $\alpha$  disk, using the background reference. The right column shows the Kiel diagram for the APOGEE sample (top right) and GALAH sample (bottom right). Again, the background gray points show the reference stars, the dark gray points show the high- $\alpha$  stars with  $-0.6 \text{ dex} < [\text{Fe}/\text{H}] < -0.4 \text{ dex}$ , and the larger points show the values from the public survey data releases for the PEPHI stars, colored by their metallicity values. Since we fixed  $\log g$  and  $T_{\text{eff}}$  while fitting the PEPHI spectra, we do not have a different set of values from our new observations. The points outlined in black show the abundance measurements for the truly young high- $\alpha$  stars that will be described in Section 3.1.

observing time to produce a predicted RV. We place an RV floor of  $100 \text{ m s}^{-1}$  for APOGEE and  $50 \text{ m s}^{-1}$  for PEPHI; any candidate with predicted variability below this limit is rejected. Based on predicted contrast, we also reject spectroscopic binaries with line-splitting (SB2s) that would appear resolved in the observed spectra. We then compare the predicted RVs to measured RVs using a  $\chi^2$  test, with the  $\chi^2$  cumulative distribution function probability taken as the rejection probability of the system. For systems with RVs from both PEPHI and APOGEE, we calculate limits using each dataset separately, as the instrumental offset could be mistaken for astrophysical variability in the RV analysis. The RV measurements from APOGEE are taken from Sayd-

jari et al. (2025), which agree with the APOGEE DR17 Doppler outputs (Nidever 2021) for our stars. We then calculate the confidence limit on the presence of a candidate companion by binning the samples in parameter space and calculating the percentage of samples that survived rejection sampling. Given the large distance to these stars, the binary signal will not have a significant impact on astrometry, so Gaia RUWE does not produce very significant constraints.

We have done this analysis for the two GALAH-K2 stars with confirmed Li measurements (03435417+1719250 and 01084954-0030464), the one APOGEE-K2 star with Li measurement (03413908+2359163), and the one APOGEE-Kepler

star with interesting features (18432994+4356589). The RVs and binary analysis results are shown in the bottom right panel in their respective figures (Figure 3-6). These figures show the 99<sup>th</sup>-percentile confidence limit — a candidate companion with a mass ratio above this line is rejected with 95% confidence. The analysis for each plot will be discussed in Section 3.

### 2.8. Abundance Comparison with Doppelgänger Stars

To understand whether there are unique patterns in the detailed chemical abundances, including planet engulfment signatures, of the likely young high- $\alpha$  stars, we compare the abundances of these stars with their doppelgängers. We do so by selecting stars that agree with the target star’s  $\log g$ ,  $T_{\text{eff}}$ , [Fe/H], and [Mg/Fe], within uncertainty. We followed the same procedure as the previous paper (Lu et al. 2025), but enforced an SNR condition so that the differences between the targeted star and the doppelgängers’ SNR values are less than 50. The SNR for GALAH ID 160110002101185, 2MASS J03435417+1719250, is 126; The SNR for GALAH ID 161006004901279, 2MASS J01084954-0030464, is 63.6. V is missing for GALAH ID 161006004901279, and Al is missing for GALAH ID 160110002101185 because there are no reported GALAH measurements. The SNR for 2MASS J18432994+4356589 is 74.6; The SNR for 2MASS J03413908+2359163 is 116.6. We did not use the abundances from PEPSI to perform this test as there are known differences between the surveys, and since we do not have PEPSI observations for the doppelgänger stars, we cannot perform a consistent comparison using abundances from PEPSI. The results are shown in the bottom left panel in each of their corresponding figures (Figure 3-6).

## 3. RESULTS

Combining abundances (Li, Mg, and Fe), rotation periods, and RV measurements, we identify three genuinely young high- $\alpha$  rotators (see Section 3.1), and one possible merger product (see Section 3.3). We will now take a look at the combined information for these four stars individually. These results are also summarized in Table 3.

### 3.1. Three Genuinely Young high- $\alpha$ Dwarfs

In this section, we will look at the three newly identified genuinely young high- $\alpha$  dwarf stars (Section 3.1.1 to Section 3.1.3) and the one possible merger (Section 3.3) identified in Section 2.6 individually. We will then discuss the age and chemical signatures the genuinely young high- $\alpha$  dwarf stars have in common in Section 3.2. Finally, we will speculate the possible formation pathways of genuinely young high- $\alpha$  stars in Section 3.4.

#### 3.1.1. 2MASS J03413908+2359163

This star has a rotation period measurement of 32.21 days, with no other strong peaks detected around the main peak in the periodogram. With its Gaia  $G_{\text{BP}} - G_{\text{RP}}$  color of 1.28, and period measurement, GPgyro (Lu et al. 2024) inferred an age of  $5.8^{+0.2}_{-0.2}$  Gyr. With additional metallicity information, STAREVOL inferred an age of  $5.1^{+0.8}_{-0.1}$  Gyr, agreeing with that from GPgyro. This is an intermediate age high- $\alpha$  star since typical high- $\alpha$  stars have ages between 7-13 Gyr (e.g., Xiang & Rix 2022; Pinsonneault et al. 2025).

This star was observed in APOGEE, with three epochs of RVs available. We performed two additional follow-ups with PEPSI. The binary analysis suggests we are able to exclude a mass ratio of  $\sim 0.4$  to the synchronized limit with APOGEE RVs. This is about  $0.34 M_{\odot}$ , using the output mass of  $0.86 M_{\odot}$  for the primary star from STAREVOL. However, if the star has a stellar companion with a mass ratio of 0.4, is it likely already synchronized by the typical age of a high- $\alpha$  star of 8 Gyr (assuming the equilibrium tide prescription using Equation 4.6 of Zahn 1977). As a result, if an actual companion exists, its mass ratio is likely less than 0.1. The binary analysis suggests this star likely does not have a stellar mass donor, and have not been spun up by close-by stellar companions. Future follow-up should focus on collecting more RV measurements to place further exclude sub-stellar companions, if one exists.

Abundance analysis shows significant Li abundance in the star’s atmosphere (see middle left panel in Figure 3), suggesting it has not gone through stellar mergers. Although one may argue planet engulfment and pollution from nearby AGB or novae can also lead to enhancement in surface Li for unevolved stars (e.g., Koch et al. 2011; Li et al. 2018; Matsuno et al. 2025), these unevolved stars discovered previously are typically metal-poor, with  $[\text{Fe}/\text{H}] < -1$  dex, and have enhancements in *s*-process elements, Na, or N, which are not seen in any of our stars. Doppelgänger analysis (bottom left panel) shows no strong trend with refractory elements or condensation temperature, suggesting no obvious signature of planet engulfment.

#### 3.1.2. 2MASS J03435417+1719250

This star has a clear rotation signal at 16.52 days, with no strong peaks at the half or double period. With its Gaia  $G_{\text{BP}} - G_{\text{RP}}$  color of 0.82, and period measurement, GPgyro (Lu et al. 2024) inferred an age of  $2.35^{+0.07}_{-0.09}$  Gyr. STAREVOL is not able to provide precise age information for this star, after combining isochrone tracks with its rotation period.

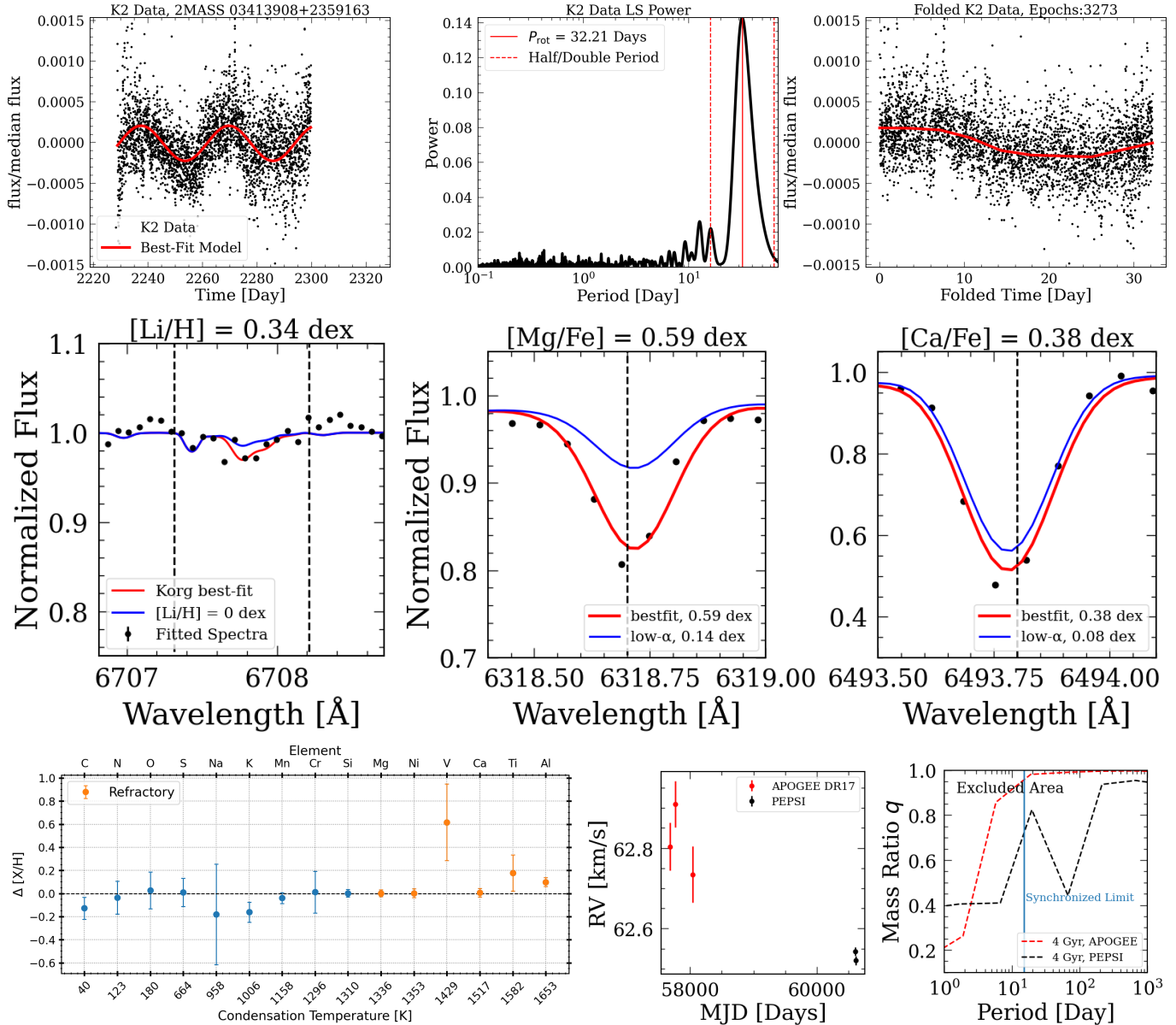


**Figure 3.** Detail analysis for 03413908+2359163. Top: K2 light curve with the best-fit model (left), the Lomb-Scargle Periodogram where the red line shows the period detected and the red dotted lines show the half and double periods (middle), and the folded light curve onto the detected period (right). Middle left: Korg best-fit model (red lines) around the Li line. The vertical black dashed lines show the window for the Li line. The black points show the PEPSI spectra for this targeted star, and the blue line shows the synthetic spectrum of a star with the same stellar parameters but with  $[\text{Li}/\text{H}] = 0$  dex. Middle right: BACCHUS best-fit model (red) to the data for the Mg 6318.7 line and the Ca 6493.8 line. The vertical dashed line shows the centers of the lines. The blue lines show the synthetic spectra of a low- $\alpha$  star with the same stellar parameters generated from BACCHUS for comparison. Bottom left: Abundance comparisons with doppelgänger stars (detail see Section 2.8). The orange points show refractory elements used to vet planet engulfment events. Bottom right: RV measurements and binary exclusion tests for this star. In the binary exclusion test plot showing mass ratio vs orbital period, the blue vertical line shows the synchronized binary limit at 15 days, binary stars with an orbital period less than 15 days should be synchronized. The lines show 95% confidence level for binary exclusion assuming a typical age of a high- $\alpha$  star of 10 Gyr, analyzed with PEPSI RVs (black) and APOGEE RVs (red) separately. The dashed lines show those for an intermediate age high- $\alpha$  star of 4 Gyr.

2MASS ID	$P_{\text{rot}}$ [Days]	Age [Gyr]	$A(\text{Li})$	Planet	Engulfment?	Stellar Companion?	$s$ -process	Enhancements?
03413908+2359163	32.21	$5.80^{+0.13}_{-0.22}$	1.39		N			N/A
03435417+1719250	16.52	$2.36^{+0.05}_{-0.11}$	1.42		N		[Ce/Fe]=1.00 dex	
01084954-0030464	20.98	$3.84^{+0.27}_{-0.19}$	2.13		N			N

**Table 3.** 2MASS ID, rotation periods, gyrochronology age inferred with **GPgyro**,  $A(\text{Li})$  measured using  $[\text{Li}/\text{H}]+1.05$ , with  $[\text{Li}/\text{H}]$  measured from **Korg**, whether the star exhibit planet engulfment signature from comparing with doppelgänger stars, whether the RV measurements show signature of a close-by stellar companion, and whether it shows enhancements in  $s$ -process elements according to PEPSI spectra analysis with **BACCHUS** (to vet for asymptotic giant branch (AGB) mass transfer). We only include values of  $s$ -process element abundances from PEPSI if  $[\text{X}/\text{Fe}] > 0.5$  dex. We are not able to measure any  $s$ -process elements for 03413908+2359163 due to the low SNR for the PEPSI spectra.

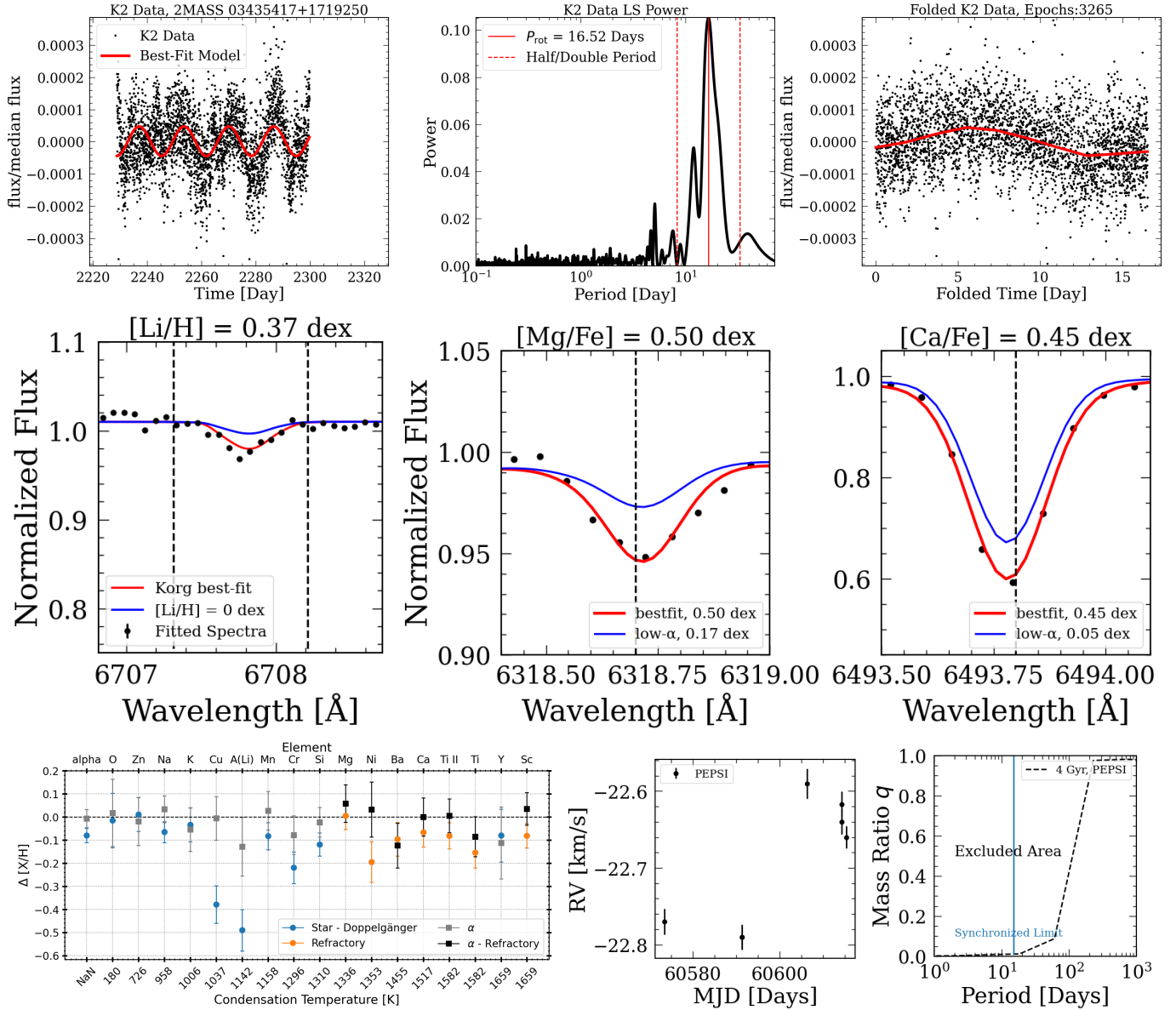


**Figure 4.** Similar as Figure 3 but for 03435417+1719250. The differences here is for the comparison with doppelgänger stars in the bottom left panel, we compared both with doppelgängers selecting on agreeing  $[\text{Mg}/\text{Fe}]$  (circle points) or agreeing  $[\alpha/\text{Fe}]$  (square points) as this star likely exhibit an abnormally high  $[\text{Mg}/\text{Fe}]$  values. This is a GALAH-K2 candidate star.

With 6 RV measurements from PEPSI, we are better able to exclude binary companions down to a mass ratio of 0.04 at the synchronized period. This mass ratio excludes a close companion over  $0.017 M_{\odot}$  (about  $17 M_{\mathrm{J}}$ ), using the output mass of  $0.83 M_{\odot}$  for the primary star from STAREVOL. As a result, no close-in companion may be able to affect its rotation period, since a hot Jupiter does not strongly affect its host star's period evolution tidally beyond 0.05 AU (e.g., Benbakoura et al. 2019).

This star also has a detectable Li abundance as shown in the middle left panel in Figure 4. Interestingly, by selecting on  $[\mathrm{Mg}/\mathrm{H}]$  as an indication for  $\alpha$  element, almost all the other  $\alpha$  elements for this star are lower compared to its doppelgängers. If this star has a slightly elevated Mg, it could account for some of the discrepancy between the element abundances. Indeed, if we select doppelgänger stars based on the overall  $\alpha$  elements, the differences in element abundances disappeared or decreased significantly, including Li and Cu, which exhibit the most obvious discrepancy when selecting doppelgängers via  $[\mathrm{Mg}/\mathrm{H}]$ . This is the only star in our genuinely young GALAH-K2 sample that does not show elevated Li abundance. This star also has the lowest metallicity compared to the rest.

### 3.1.3. 2MASS J01084954-0030464

Period detection for this star has the strongest peak at 20.98 days (see top middle panel from Figure 5), which yields an age of  $3.9^{+0.3}_{-0.2}$  Gyr with GPgyro. Again, with its unique combination of stellar parameters, STAREVOL is not able to provide precise age information for this star. However, a possible peak exists around double the period at 40 days. If the second highest peak is the true period ( $\sim 35$  days), this star would be  $11.9^{+1.8}_{-1.4}$  Gyr according to GPgyro, which matches with that of a normal high- $\alpha$  star.

This star shows an elevated Li abundance compared to its doppelgänger stars (bottom left panel in Figure 5), and binary analysis suggests no high mass companions (mass ratio  $> 0.5$ ) exist within an orbital period of 100 days. No strong trend differences in abundances exist besides Li. However, a possible positive slope exists with condensation temperature for refractory elements as shown in the bottom left panel of Figure 5. This trend, if real, could suggest a recent planet engulfment event (e.g., Ramírez et al. 2009; Teske et al. 2016; Meléndez et al. 2017; Spina et al. 2021). Moreover, it has a relatively high  $[\mathrm{Ce}/\mathrm{Fe}]$  measurement of 1.0 dex, suggesting possible AGB mass transfer. However, this is unlikely as we do not see any nearby stellar companion.

## 3.2. Patterns in Element Abundances for Genuinely Young high- $\alpha$ Dwarfs

Combining the other genuinely young high- $\alpha$  dwarfs from Lu et al. (2025), we are able to compare their abundances with the doppelgänger stars for these four stars altogether, in order to understand whether they exhibit unique chemical patterns. Note, the comparisons are done in their respective surveys (i.e., if the targeted star is in GALAH, we select doppelgänger stars only from GALAH and compare abundances from the GALAH survey) to avoid biases across surveys.

Figure 6 top plot shows the combined element comparisons for these four stars with respect to the doppelgängers. For 03435417+1719250, we used the doppelgänger stars selected with  $\alpha$  instead of  $[\mathrm{Mg}/\mathrm{H}]$  as this star likely has elevated  $[\mathrm{Mg}/\mathrm{H}]$  values (see Section 3.1). The elements are ordered in decreasing average difference after accounting for the combined uncertainty. To do so, we first calculated the absolute value of the average difference ( $|\Delta[\mathrm{X}/\mathrm{H}]_{\mathrm{comb}}|$ ), we then divided it by the average uncertainty ( $\sigma_{\mathrm{comb}}$ ), calculated by adding the uncertainties for individual stars in quadrature. The elements are then ordered by decreasing in  $|\Delta[\mathrm{X}/\mathrm{H}]_{\mathrm{comb}}|/\sigma_{\mathrm{comb}}$ , as shown as the top axis. The gray line shows the average difference,  $\Delta[\mathrm{X}/\mathrm{H}]_{\mathrm{comb}}$ , for each element.

The difference in most  $\alpha$  elements (e.g., Ti, Ca, Ni, Mg, O) is the smallest among all stars, which is a sanity check as we selected stars that have  $[\mathrm{Mg}/\mathrm{H}]$  or  $[\alpha/\mathrm{H}]$  agreeing within uncertainty to be the doppelgänger stars. The most interesting elements are Li and Al, where out of the three GALAH-K2 stars with Li measurements from Wang et al. (2024), two stars have similar elevated Li measurements, about 0.5 dex, above their doppelgängers. All three out of four stars with Al measurements also exhibit a similar amount of slightly elevated  $[\mathrm{Al}/\mathrm{H}]$  values compared to their doppelgängers. Besides Li and Al, some other abundances, such as V, Ba, and Cu, also show some variations compared to the doppelgängers. However, it is worth pointing out that V is difficult to measure, and it is often unreliable in GALAH. In the future, we plan on proposing for PEPSI time to observe the doppelgänger stars for a more in depth comparison.

The middle row of Figure 6 shows the  $[\mathrm{Fe}/\mathrm{H}]$ -age and  $[\mathrm{Mg}/\mathrm{Fe}]$ -age relation for all the dwarf stars in APOGEE DR17 with period measurements in the background gray points, and the colored symbols show the genuinely young high- $\alpha$  dwarf stars we have identified, with the colors and symbols as indicated in the legend in the top figure. The ages are determined using GPgyro. The bottom left plot shows the Li-age relation for solar twin

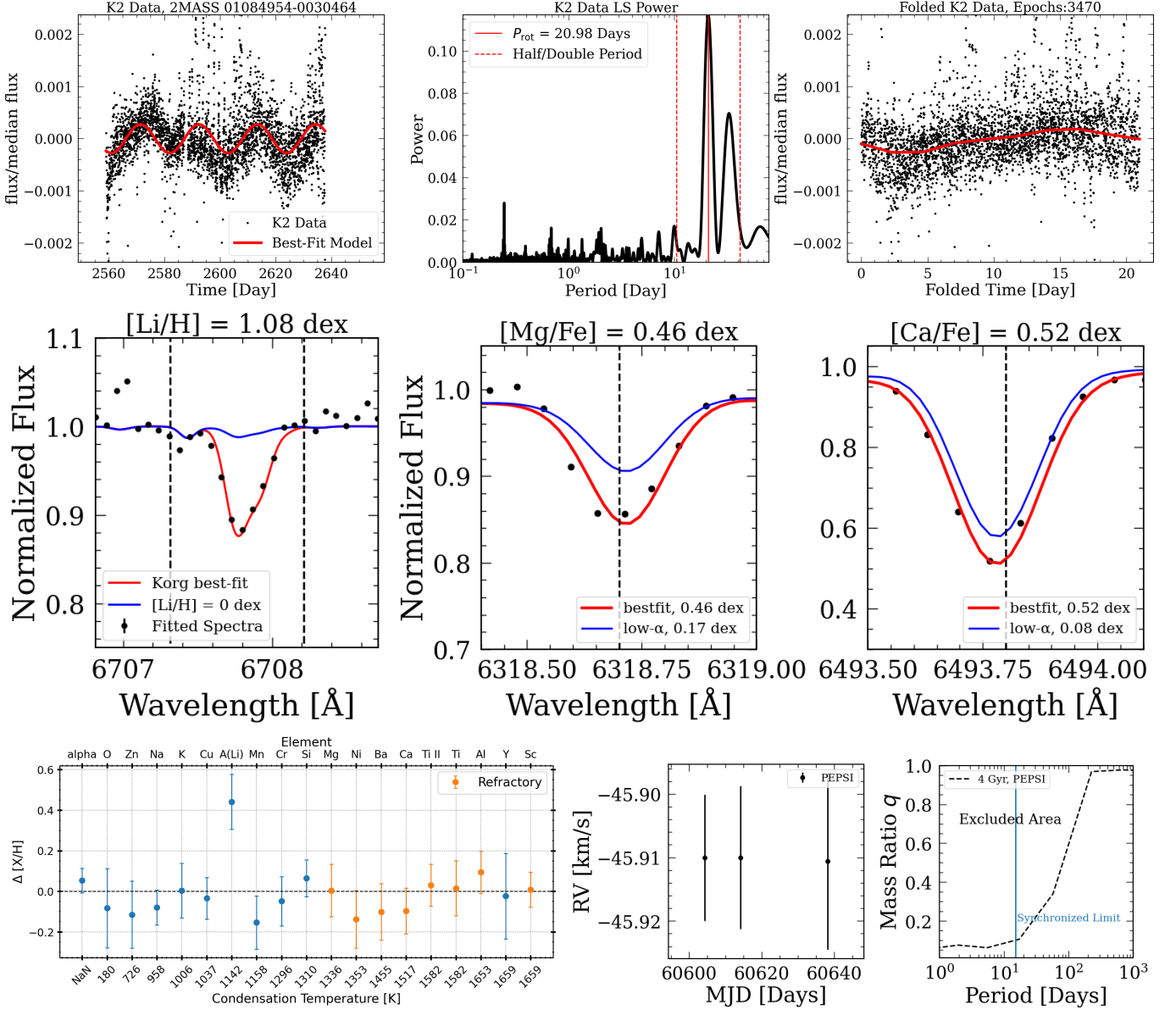


**Figure 5.** Similar as Figure 3 but for 01084954-0030464. Here we use the Ca 6439.1 line. This is a GALAH-K2 candidate star.

stars (Carlos et al. 2016). The ages in their sample is derived from isochrone fitting (Nissen 2015), and the Li abundances are measured using HARPS spectra (Mayor et al. 2003). Despite the differences in age derivation techniques and the instruments being used to derive abundances, the four genuinely young high- $\alpha$  stars follow the typical Li-age trend of solar twins of intermediate ages. One caveat is that these solar twins are near solar metallicity, and our sample has a metallicity of  $\sim -0.5$  dex. However, for their high- $\alpha$  star sample, only upper limit for  $A(Li) < 0.9$  dex is detected, unlike the solar-mass stars in our sample. As a result, this comparison suggests the Li content for the genuinely young high- $\alpha$  stars likely have not been altered from

mass-transfers from a stellar or sub-stellar companion. The bottom right plot shows the  $[Al/Fe]$ - $[Fe/H]$  relation for all the high- $\alpha$  dwarf stars in APOGEE DR17, as shown in the background histogram for reference, and the white outlined colored symbols show the three genuinely young high- $\alpha$  dwarf stars, with Al measurements missing for 03435417+1719250. Interestingly enough, the stars with common abundance patterns (elevated Al and Li compared to their doppelgängers) all clustered around a metallicity of  $\sim -0.5$  dex and age about 5 Gyr. Their  $[Al/Fe]$ - $[Fe/H]$  abundances also trace the outer edge of the distribution, where stars are not common. However, since the star formation efficiency in Sagittarius is low, the  $\alpha$  abundances, including Mg and

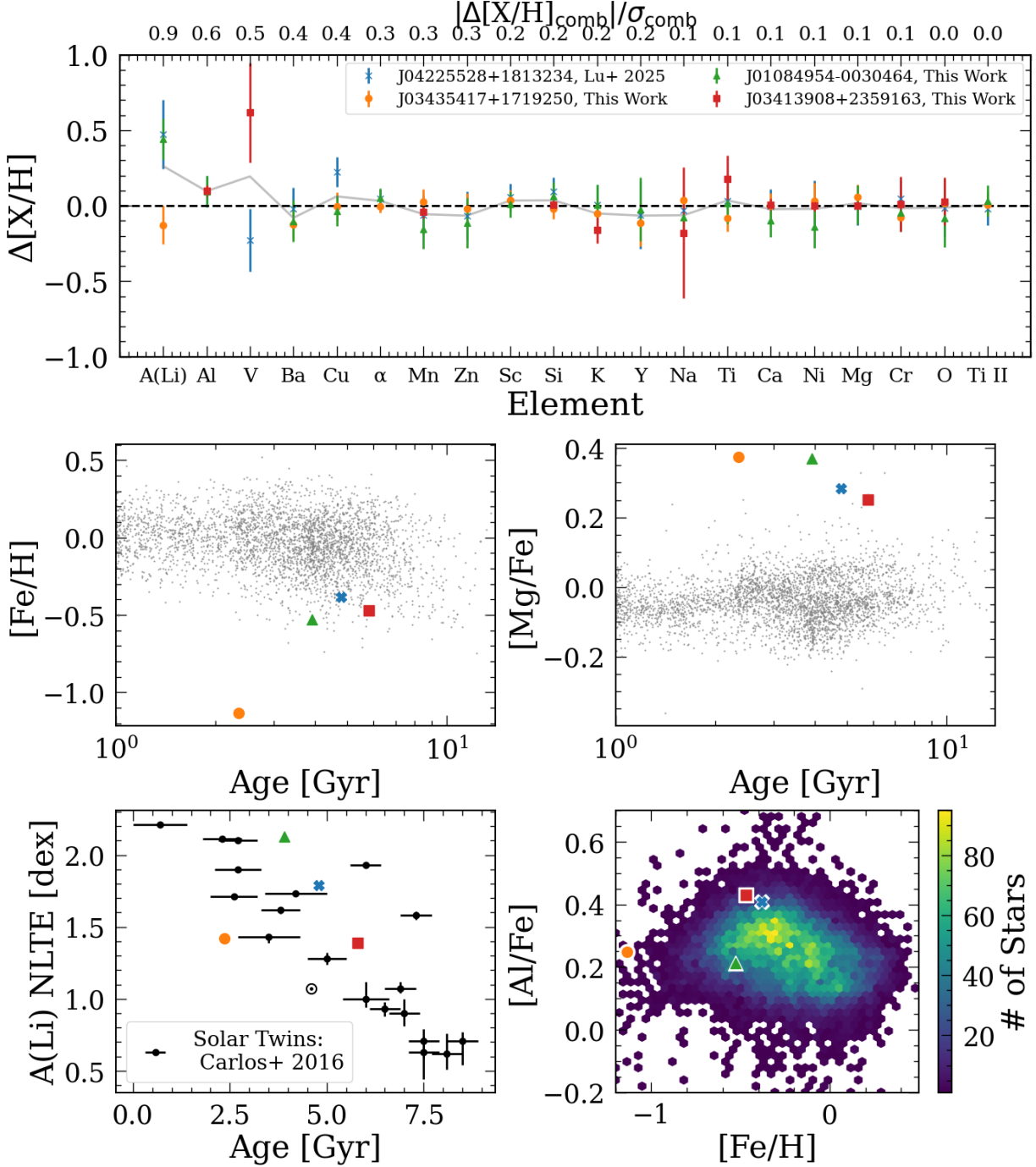


**Figure 6.** Top Row: combined element abundance difference between each genuinely young high- $\alpha$  dwarf star and its doppelgängers ordered by decreasing absolute average differences, normalized by the average uncertainty (shown as the top axis). The gray line shows the average differences for each element. Interestingly enough, three out of four stars are  $\sim 0.1$  dex elevated in [Al/H] compared to their doppelgängers, except 03435417+1719250. Two of the three stars in GALAH have Li measurements about 0.5 dex higher than their doppelgängers. Middle Row: [Fe/H]-age and [Mg/Fe]-age relation for all rotating dwarf stars in APOGEE DR17 (gray) with ages determined from Lu et al. (2024), and the four genuinely young high- $\alpha$  dwarf star (colored symbols, as indicated in the caption in the top plot). Bottom left: Li abundance as a function of age for solar twins taken from Carlos et al. (2016) shown in the black points, and our sample of 4 stars are shown in color points, and the Sun (“ $\odot$ ” symbol) is also shown. Our 4 stars except 03435417+1719250 follow the expected Li-age trend, suggesting the Li content of these stars has likely not been altered by binary mass transfer. This may be due to the fact that 03435417+1719250 has a significantly lower measured metallicity. Bottom right: [Al/Fe]-[Fe/H] relation for all the high- $\alpha$  dwarf stars in APOGEE DR17 ( $\log g > 4$ ,  $T_{\text{eff}}$  between 4500 and 6500 K, with no flags) in the background histogram, and the colored points with white outlines are the three out of four genuinely young high- $\alpha$  dwarf star. Al measurement is missing for 03435417+1719250 in GALAH DR3, and as a result, we adopted the value calculated from BACCHUS.

Al, for stars in the Sagittarius core are much lower than those of our genuinely young high- $\alpha$  dwarf stars. As a result, we do not draw any conclusions given the small sample of our stars. Hopefully, future follow-up for more young high- $\alpha$  candidates will increase the sample size and aid our understanding of this population and formation pathway.

### 3.3. One Possible Mass-Transfer Product

2MASS J18432994+4356589 shows a strong spot modulation signature based on Kepler data (see Figure 7 top two rows), visible emission in the high- $\alpha$  line core (see Figure 7 middle row, middle panel). The period for this star changes slightly between 24 and 26 days, matching what is expected for spot modulation due to differential rotation on the surface. Both high- $\alpha$  emission and strong spot modulation suggest its youth. However, its high- $\alpha$  nature suggests it should not have a strong activity signal. Since this star has a  $\log g$  of 3.6, the activity signal is likely generated with a combination of the convection zone deepens and a relatively fast rotation.

We suspect this star has gone through stellar mass transfer or merger. This star does not have a detectable Li line (see Figure 7 middle left plot), suggesting either its Li has already been destroyed during its natural evolutionary process, or a mass transfer event happened and heated the star enough to burn its Li. Since this star is evolved, it is entering the regime where Li is destroyed as the temperature at the base of the convective region becomes high enough when it ascends to the giant phase, so it is difficult to confirm whether it has gone through a mass transfer event. Moreover, the limited RV measurements from APOGEE also do not exclude a binary companion. However, since this star has a rotation period of over 20 days, it is likely not in a synchronized binary system. Future RV follow-ups will be able to provide better constraints on whether this star has a binary companion.

The abundance comparison for this star shows strong disagreement between Ti and TiII measurements from APOGEE, suggesting possible incorrect  $\log g$  measurements, since by design, the ASPCAP pipeline (Abdurro'uf et al. 2022) should return similar values for both. As a result, we are not surprised by the abundance variation compared to its doppelgänger stars.

Even though this star cannot be confirmed to be a genuinely young high- $\alpha$  star, further follow-up observations can still yield interesting results on the formation pathway of high- $\alpha$  stars with activity signatures indicating youth.

### 3.4. Formation pathways for genuinely young high- $\alpha$ stars

From these four stars, it is difficult to draw definitive conclusions on the formation pathways of genuinely young high- $\alpha$  stars, but it is likely they formed in local, self-enriched environments before the enriched gas is dispersed in the Galaxy. For example, the chemical evolution model described in Johnson et al. (2021) has predicted these stars, mostly formed in the outer disk, caused by highly variable SN Ia rate in the outer Galaxy due to sudden stellar migration of a sub-population of stars (Dubay et al. 2024). These stars exhibit similar chemical abundance patterns in  $[\alpha/\text{Fe}]$  and  $[\text{Fe}/\text{H}]$ , in that they are the most metal-poor star for their age, with moderately elevated  $\alpha$  ( $\sim 0.1$  dex). The elevated Al could also indicate possible processes happening in globular clusters, as stars in globular clusters also exhibit elevated Al compared to predictions from chemical evolution models (e.g., Sit et al. 2024; Mészáros et al. 2020). However, it is worth pointing out there is a metallicity dependence in Al enhancements produced by H-burning Mg-Al chain (e.g., Kobayashi et al. 2006; Mészáros et al. 2020), since our stars have  $[\text{Fe}/\text{H}] > -1.5$  dex, the self-enrichment happening in globular clusters is likely not significant in the metallicity range of our stars.

## 4. CONCLUSION & FUTURE WORK

We performed high-resolution spectroscopic follow-up of 4 APOGEE-Kepler, 5 APOGEE-K2, and 4 GALAH-K2 young high- $\alpha$  dwarf star candidates using PEPSI on LBT. Of the 13 observed stars, we have excluded 1 star with high- $\alpha$  but low Mg measurement from APOGEE, indicating incorrect stellar parameters or abundance measurements. This also means we are not able to confirm it belongs to the high- $\alpha$  disk. We also excluded 1 other star with a rotation period suggesting it could be similar age of a typical high- $\alpha$  star. Of the remaining 11 stars, 3 stars (2 from GALAH-K2 and 1 from APOGEE-K2) pass our additional tests on their young age, detectable lithium abundance, and low chance of a significant binary companion.

Combing with the one genuinely young high- $\alpha$  dwarf star found in Lu et al. (2025), we found:

- Two out of three in GALAH have similar elevated Li abundances,  $\Delta A(\text{Li}) \sim 0.5$  dex, compared to their doppelgänger stars, suggesting they have not gone through binary mass transfer and their youth.
- three out of four stars have similar elevated Al abundances,  $\Delta [\text{Al}/\text{Fe}] \sim 0.1$  dex, compared to their doppelgänger stars, suggesting their common chemical signature and thus, formation pathway.

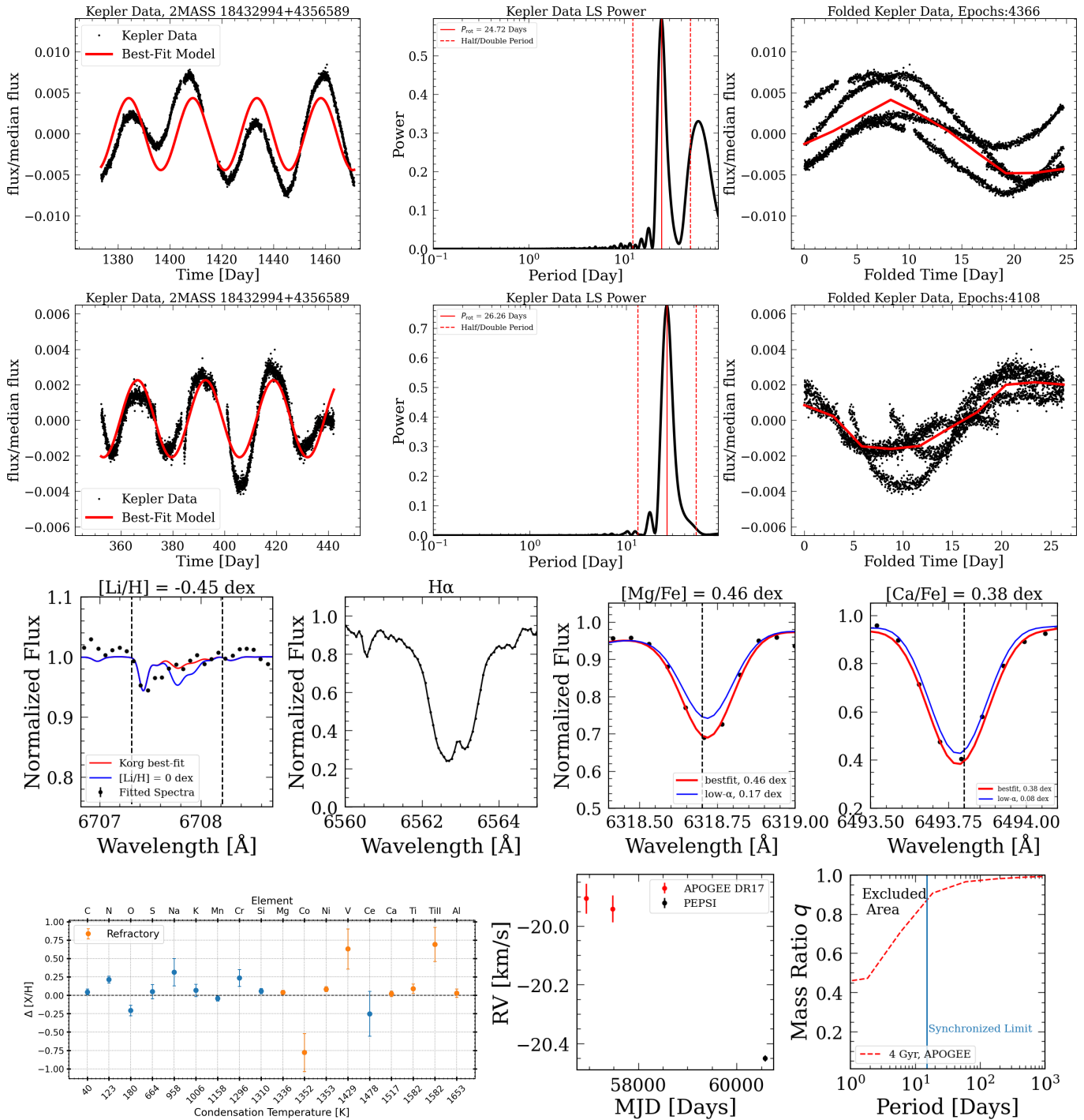


**Figure 7.** Similar as Figure 3 but for 18432994+4356589. We added the data around the H $\alpha$  line (see panel between the fits to Li and Mg in the middle row) to show the emission, indicating activity in this star. This is an APOGEE-Kepler candidate star. Since this star is in the Kepler field, multiple sectors are available for rotation period measurements. We plotted two different Kepler sectors and their rotation analysis for this star in the top two rows.

- three out of four stars are clustered at  $[\text{Fe}/\text{H}] = -0.5$  dex, with ages close to 5 Gyr. However, these stars are higher in  $\alpha$  abundances (e.g., Mg and Al) compared to the stars in the core of Sagittarius, as the star formation efficiency in Sagittarius is low.

Our key result is that the young high- $\alpha$  phenomenon is not restricted to asteroseismic mass measurements in giants. There are real cases where all of the available evidence points to youth; the stars that we have identified would not have been classified as old, or unusual, except relative to expectations for their high  $[\alpha/\text{Fe}]$  ratio. It is also undoubtedly true that many apparently young candidates are the products of stellar interactions. Moving forward, we therefore believe that this should be treated as a mixed population, and effort should be made to distinguish between both of these interesting families of objects. Future spectra and multi-epoch RV follow-ups should confirm more genuinely young  $\alpha$  dwarf stars. Moreover, asteroseismic constrain from the PLATO mission (Rauer et al. 2014) could also put additional constrain on the ages of these stars. With more detections of genuinely young  $\alpha$  stars, we will be able to better understand their formation pathway.

## 5. ACKNOWLEDGMENTS

Y.L. would like to thank the helpful inputs from the OSU Galaxy Group and Stars Group. Observations have benefited from the use of ALTA Center (alta.arcetri.inaf.it) forecasts performed with the Astro-Meso-Nh model. Initialization data of the ALTA automatic forecast system come from the General Circulation Model (HRES) of the European Centre for Medium Range Weather Forecasts. This work has made use of data from the European Space Agency (ESA) mission Gaia,<sup>2</sup> processed by the Gaia Data Processing and Analysis Consortium (DPAC).<sup>3</sup> Funding for the DPAC

has been provided by national institutions, in particular the institutions participating in the Gaia Multilateral Agreement. This research also made use of public auxiliary data provided by ESA/Gaia/DPAC/CU5 and prepared by Carine Babusiaux. All the Kepler and K2 data used in this paper can be found in MAST: [10.17909/T9059R](https://doi.org/10.17909/T9059R) and [10.17909/T93W28](https://doi.org/10.17909/T93W28) (STScI 2011, 2016). Parts of the text and analysis were assisted by OpenAI’s ChatGPT (version GPT-4.5, accessed July 2025) for drafting and editing support. SB acknowledges support from the Australian Research Council under grant number DE240100150. LA acknowledges support from the Swiss National Science Foundation (SNF; Project 200021L-231331) and the French Agence Nationale de la Recherche (ANR-24-CE93-0009-01) “PRIMA - PRobing the origIns of the Milky WAY’s oldest stars”. CM is supported by the NSF Astronomy and Astrophysics Fellowship award number AST-2401638.

This research has also made use of NASA’s Astrophysics Data System, and the VizieR (Ochsenbein et al. 2000) and SIMBAD (Wenger et al. 2000) databases, operated at CDS, Strasbourg, France.

*Facilities:* LBT, PEPSI, Gaia, Kepler, K2, APOGEE, GALAH

*Software:* BACCHUS (Masseron et al. 2016), Astropy (Astropy Collaboration et al. 2013; Price-Whelan et al. 2018; Astropy Collaboration et al. 2022), lightkurve (Lightkurve Collaboration et al. 2018), Matplotlib (Hunter 2007), NumPy (Harris et al. 2020), Pandas (McKinney et al. 2010), gala (Price-Whelan 2017), galpy (Bovy 2015), seaborn (Waskom 2021), The Joker (Price-Whelan et al. 2017), ChatGPT (OpenAI 2025), Korg (Wheeler et al. 2023), GPgyro (Lu et al. 2024), STAREVOL (Amard et al. 2019)

## REFERENCES

Abdurro’uf, Accetta, K., Aerts, C., et al. 2022, ApJS, 259, 35, doi: [10.3847/1538-4365/ac4414](https://doi.org/10.3847/1538-4365/ac4414)

Amard, L., Palacios, A., Charbonnel, C., et al. 2019, A&A, 631, A77, doi: [10.1051/0004-6361/201935160](https://doi.org/10.1051/0004-6361/201935160)

Asplund, M., Grevesse, N., Sauval, A. J., & Scott, P. 2009, ARA&A, 47, 481, doi: [10.1146/annurev.astro.46.060407.145222](https://doi.org/10.1146/annurev.astro.46.060407.145222)

Astropy Collaboration, Robitaille, T. P., Tollerud, E. J., et al. 2013, A&A, 558, A33, doi: [10.1051/0004-6361/201322068](https://doi.org/10.1051/0004-6361/201322068)

Astropy Collaboration, Price-Whelan, A. M., Lim, P. L., et al. 2022, ApJ, 935, 167, doi: [10.3847/1538-4357/ac7c74](https://doi.org/10.3847/1538-4357/ac7c74)

Barnes, S. A. 2003, ApJ, 586, 464, doi: [10.1086/367639](https://doi.org/10.1086/367639)

Bedell, M., Meléndez, J., Bean, J. L., et al. 2014, ApJ, 795, 23, doi: [10.1088/0004-637X/795/1/23](https://doi.org/10.1088/0004-637X/795/1/23)

Benbakoura, M., Réville, V., Brun, A. S., Le Poncin-Lafitte, C., & Mathis, S. 2019, A&A, 621, A124, doi: [10.1051/0004-6361/201833314](https://doi.org/10.1051/0004-6361/201833314)

<sup>2</sup> <https://www.cosmos.esa.int/gaia>

<sup>3</sup> <https://www.cosmos.esa.int/web/gaia/dpac/consortium>

Blanco-Cuaresma, S., Soubiran, C., Heiter, U., & Jofré, P. 2014, A&A, 569, A111, doi: [10.1051/0004-6361/201423945](https://doi.org/10.1051/0004-6361/201423945)

Borucki, W. J., Koch, D., Basri, G., et al. 2010, Science, 327, 977, doi: [10.1126/science.1185402](https://doi.org/10.1126/science.1185402)

Bovy, J. 2015, ApJS, 216, 29, doi: [10.1088/0067-0049/216/2/29](https://doi.org/10.1088/0067-0049/216/2/29)

Buder, S., Sharma, S., Kos, J., et al. 2021, MNRAS, 506, 150, doi: [10.1093/mnras/stab1242](https://doi.org/10.1093/mnras/stab1242)

Byrom, S., & Tayar, J. 2024, Research Notes of the American Astronomical Society, 8, 201, doi: [10.3847/2515-5172/ad7093](https://doi.org/10.3847/2515-5172/ad7093)

Carlos, M., Nissen, P. E., & Meléndez, J. 2016, A&A, 587, A100, doi: [10.1051/0004-6361/201527478](https://doi.org/10.1051/0004-6361/201527478)

Cerqui, V., Haywood, M., Di Matteo, P., Katz, D., & Royer, F. 2023, A&A, 676, A108, doi: [10.1051/0004-6361/202346334](https://doi.org/10.1051/0004-6361/202346334)

Chiappini, C., Anders, F., Rodrigues, T. S., et al. 2015, A&A, 576, L12, doi: [10.1051/0004-6361/201525865](https://doi.org/10.1051/0004-6361/201525865)

Claytor, Z. R., van Saders, J. L., Santos, Á. R. G., et al. 2020, ApJ, 888, 43, doi: [10.3847/1538-4357/ab5c24](https://doi.org/10.3847/1538-4357/ab5c24)

Conroy, C., Weinberg, D. H., Naidu, R. P., et al. 2022, arXiv e-prints, arXiv:2204.02989, doi: [10.48550/arXiv.2204.02989](https://doi.org/10.48550/arXiv.2204.02989)

Das, P., Hawkins, K., & Jofré, P. 2020, MNRAS, 493, 5195, doi: [10.1093/mnras/stz3537](https://doi.org/10.1093/mnras/stz3537)

De Silva, G. M., Freeman, K. C., Bland-Hawthorn, J., et al. 2015, MNRAS, 449, 2604, doi: [10.1093/mnras/stv327](https://doi.org/10.1093/mnras/stv327)

Dubay, L. O., Johnson, J. A., & Johnson, J. W. 2024, ApJ, 973, 55, doi: [10.3847/1538-4357/ad61df](https://doi.org/10.3847/1538-4357/ad61df)

Garver, B. R., Nidever, D. L., Debattista, V. P., Bernaldo e Silva, L., & Khachaturyants, T. 2023, ApJ, 953, 128, doi: [10.3847/1538-4357/acdfc6](https://doi.org/10.3847/1538-4357/acdfc6)

Green, G. 2018, The Journal of Open Source Software, 3, 695, doi: [10.21105/joss.00695](https://doi.org/10.21105/joss.00695)

Green, G. M., Schlafly, E., Zucker, C., Speagle, J. S., & Finkbeiner, D. 2019, ApJ, 887, 93, doi: [10.3847/1538-4357/ab5362](https://doi.org/10.3847/1538-4357/ab5362)

Green, G. M., Schlafly, E. F., Finkbeiner, D., et al. 2018, MNRAS, 478, 651, doi: [10.1093/mnras/sty1008](https://doi.org/10.1093/mnras/sty1008)

Grevesse, N., Asplund, M., & Sauval, A. J. 2007, SSRv, 130, 105, doi: [10.1007/s11214-007-9173-7](https://doi.org/10.1007/s11214-007-9173-7)

Grisoni, V., Chiappini, C., Miglio, A., et al. 2024, A&A, 683, A111, doi: [10.1051/0004-6361/202347440](https://doi.org/10.1051/0004-6361/202347440)

Gustafsson, B., Edvardsson, B., Eriksson, K., et al. 2008, A&A, 486, 951, doi: [10.1051/0004-6361:200809724](https://doi.org/10.1051/0004-6361:200809724)

Harris, C. R., Millman, K. J., van der Walt, S. J., et al. 2020, Nature, 585, 357, doi: [10.1038/s41586-020-2649-2](https://doi.org/10.1038/s41586-020-2649-2)

Hayes, C. R., Masseron, T., Sobeck, J., et al. 2022, ApJS, 262, 34, doi: [10.3847/1538-4365/ac839f](https://doi.org/10.3847/1538-4365/ac839f)

Heiter, U., Lind, K., Bergemann, M., et al. 2021, A&A, 645, A106, doi: [10.1051/0004-6361/201936291](https://doi.org/10.1051/0004-6361/201936291)

Hekker, S., & Johnson, J. A. 2019, MNRAS, 487, 4343, doi: [10.1093/mnras/stz1554](https://doi.org/10.1093/mnras/stz1554)

Hill, J. M., Green, R. F., Ashby, D. S., et al. 2012, in Society of Photo-Optical Instrumentation Engineers (SPIE) Conference Series, Vol. 8444, Ground-based and Airborne Telescopes IV, ed. L. M. Stepp, R. Gilmozzi, & H. J. Hall, 84441A, doi: [10.1117/12.926636](https://doi.org/10.1117/12.926636)

Howell, S. B., Sobeck, C., Haas, M., et al. 2014, PASP, 126, 398, doi: [10.1086/676406](https://doi.org/10.1086/676406)

Hunter, J. D. 2007, Computing in Science & Engineering, 9, 90, doi: [10.1109/MCSE.2007.55](https://doi.org/10.1109/MCSE.2007.55)

Husser, T. O., Wende-von Berg, S., Dreizler, S., et al. 2013, A&A, 553, A6, doi: [10.1051/0004-6361/201219058](https://doi.org/10.1051/0004-6361/201219058)

Izzard, R. G., Preece, H., Jofré, P., et al. 2018, MNRAS, 473, 2984, doi: [10.1093/mnras/stx2355](https://doi.org/10.1093/mnras/stx2355)

Jofré, P., Jorissen, A., Van Eck, S., et al. 2016, A&A, 595, A60, doi: [10.1051/0004-6361/201629356](https://doi.org/10.1051/0004-6361/201629356)

Jofré, P., Jorissen, A., Aguilera-Gómez, C., et al. 2023, A&A, 671, A21, doi: [10.1051/0004-6361/202244524](https://doi.org/10.1051/0004-6361/202244524)

Johnson, J. W., Weinberg, D. H., Vincenzo, F., et al. 2021, MNRAS, 508, 4484, doi: [10.1093/mnras/stab2718](https://doi.org/10.1093/mnras/stab2718)

Jones, B. F., Fischer, D., & Soderblom, D. R. 1999, AJ, 117, 330, doi: [10.1086/300664](https://doi.org/10.1086/300664)

Kobayashi, C., Umeda, H., Nomoto, K., Tominaga, N., & Ohkubo, T. 2006, ApJ, 653, 1145, doi: [10.1086/508914](https://doi.org/10.1086/508914)

Koch, A., Lind, K., & Rich, R. M. 2011, ApJL, 738, L29, doi: [10.1088/2041-8205/738/2/L29](https://doi.org/10.1088/2041-8205/738/2/L29)

Kurucz, R. L. 1992, in The Stellar Populations of Galaxies, ed. B. Barbuy & A. Renzini, Vol. 149, 225

Li, H., Aoki, W., Matsuno, T., et al. 2018, ApJL, 852, L31, doi: [10.3847/2041-8213/aaa438](https://doi.org/10.3847/2041-8213/aaa438)

Lightkurve Collaboration, Cardoso, J. V. d. M., Hedges, C., et al. 2018, Lightkurve: Kepler and TESS time series analysis in Python, Astrophysics Source Code Library, <http://ascl.net/1812.013>

Lu, Y., Angus, R., Foreman-Mackey, D., & Hattori, S. 2024, AJ, 167, 159, doi: [10.3847/1538-3881/ad28b9](https://doi.org/10.3847/1538-3881/ad28b9)

Lu, Y., Colman, I. L., Sayeed, M., et al. 2025, AJ, 169, 168, doi: [10.3847/1538-3881/ada9e0](https://doi.org/10.3847/1538-3881/ada9e0)

Lurie, J. C., Vyhmeister, K., Hawley, S. L., et al. 2017, AJ, 154, 250, doi: [10.3847/1538-3881/aa974d](https://doi.org/10.3847/1538-3881/aa974d)

Majewski, S. R., Schiavon, R. P., Frinchaboy, P. M., et al. 2017, AJ, 154, 94, doi: [10.3847/1538-3881/aa784d](https://doi.org/10.3847/1538-3881/aa784d)

Manea, C., Ness, M., Hawkins, K., et al. 2025, arXiv e-prints, arXiv:2508.16717, doi: [10.48550/arXiv.2508.16717](https://doi.org/10.48550/arXiv.2508.16717)

Martig, M., Rix, H.-W., Silva Aguirre, V., et al. 2015, MNRAS, 451, 2230, doi: [10.1093/mnras/stv1071](https://doi.org/10.1093/mnras/stv1071)

Masseron, T., Merle, T., & Hawkins, K. 2016, BACCHUS: Brussels Automatic Code for Characterizing High accuracy Spectra, Astrophysics Source Code Library, record ascl:1605.004

Masseron, T., Plez, B., Van Eck, S., et al. 2014, *A&A*, 571, A47, doi: [10.1051/0004-6361/201423956](https://doi.org/10.1051/0004-6361/201423956)

Matsuno, T., Kemp, A., Tanikawa, A., et al. 2025, *A&A*, 699, A171, doi: [10.1051/0004-6361/202554264](https://doi.org/10.1051/0004-6361/202554264)

Mayor, M., Pepe, F., Queloz, D., et al. 2003, *The Messenger*, 114, 20

McKinney, W., et al. 2010, in Proceedings of the 9th Python in Science Conference, Vol. 445, Austin, TX, 51–56

Meibom, S., & Mathieu, R. D. 2005, in Astronomical Society of the Pacific Conference Series, Vol. 333, Tidal Evolution and Oscillations in Binary Stars, ed. A. Claret, A. Giménez, & J. P. Zahn, 95

Meléndez, J., Bedell, M., Bean, J. L., et al. 2017, *A&A*, 597, A34, doi: [10.1051/0004-6361/201527775](https://doi.org/10.1051/0004-6361/201527775)

Mészáros, S., Masseron, T., García-Hernández, D. A., et al. 2020, *MNRAS*, 492, 1641, doi: [10.1093/mnras/stz3496](https://doi.org/10.1093/mnras/stz3496)

Ness, M., Hogg, D. W., Rix, H. W., Ho, A. Y. Q., & Zasowski, G. 2015, *ApJ*, 808, 16, doi: [10.1088/0004-637X/808/1/16](https://doi.org/10.1088/0004-637X/808/1/16)

Nidever, D. 2021, dnidever/doppler: Cannon and Payne models, v1.1.0, Zenodo, doi: [10.5281/zenodo.4906681](https://doi.org/10.5281/zenodo.4906681)

Nissen, P. E. 2015, *A&A*, 579, A52, doi: [10.1051/0004-6361/201526269](https://doi.org/10.1051/0004-6361/201526269)

Ochsenbein, F., Bauer, P., & Marcout, J. 2000, *A&AS*, 143, 23, doi: [10.1051/aas:2000169](https://doi.org/10.1051/aas:2000169)

OpenAI. 2025, ChatGPT (July 2025 version), <https://chat.openai.com>

Pinsonneault, M. H., Steigman, G., Walker, T. P., & Narayanan, V. K. 2002, *ApJ*, 574, 398, doi: [10.1086/340119](https://doi.org/10.1086/340119)

Pinsonneault, M. H., Zinn, J. C., Tayar, J., et al. 2025, *ApJS*, 276, 69, doi: [10.3847/1538-4365/ad9fef](https://doi.org/10.3847/1538-4365/ad9fef)

Plez, B. 2012, Turbospectrum: Code for spectral synthesis, Astrophysics Source Code Library, record ascl:1205.004

Price-Whelan, A. M. 2017, *The Journal of Open Source Software*, 2, 388, doi: [10.21105/joss.00388](https://doi.org/10.21105/joss.00388)

Price-Whelan, A. M., Hogg, D. W., Foreman-Mackey, D., & Rix, H.-W. 2017, *ApJ*, 837, 20, doi: [10.3847/1538-4357/aa5e50](https://doi.org/10.3847/1538-4357/aa5e50)

Price-Whelan, A. M., Sipőcz, B. M., Günther, H. M., et al. 2018, *AJ*, 156, 123, doi: [10.3847/1538-3881/aabc4f](https://doi.org/10.3847/1538-3881/aabc4f)

Ramírez, I., Meléndez, J., & Asplund, M. 2009, *A&A*, 508, L17, doi: [10.1051/0004-6361/200913038](https://doi.org/10.1051/0004-6361/200913038)

Rauer, H., Catala, C., Aerts, C., et al. 2014, *Experimental Astronomy*, 38, 249, doi: [10.1007/s10686-014-9383-4](https://doi.org/10.1007/s10686-014-9383-4)

Ryan, S. G., Beers, T. C., Kajino, T., & Rosolankova, K. 2001, *ApJ*, 547, 231, doi: [10.1086/318338](https://doi.org/10.1086/318338)

Ryan, S. G., Gregory, S. G., Kolb, U., Beers, T. C., & Kajino, T. 2002, *ApJ*, 571, 501, doi: [10.1086/339939](https://doi.org/10.1086/339939)

Saydjari, A. K., Finkbeiner, D. P., Wheeler, A. J., et al. 2025, *AJ*, 169, 167, doi: [10.3847/1538-3881/adb02d](https://doi.org/10.3847/1538-3881/adb02d)

Silva Aguirre, V., Bojsen-Hansen, M., Slumstrup, D., et al. 2018, *MNRAS*, 475, 5487, doi: [10.1093/mnras/sty150](https://doi.org/10.1093/mnras/sty150)

Simonian, G. V. A., Pinsonneault, M. H., & Terndrup, D. M. 2019, *ApJ*, 871, 174, doi: [10.3847/1538-4357/aaf97c](https://doi.org/10.3847/1538-4357/aaf97c)

Sit, T., Weinberg, D. H., Wheeler, A., et al. 2024, *ApJ*, 970, 180, doi: [10.3847/1538-4357/ad4ed2](https://doi.org/10.3847/1538-4357/ad4ed2)

Spina, L., Sharma, P., Meléndez, J., et al. 2021, *Nature Astronomy*, 5, 1163, doi: [10.1038/s41550-021-01451-8](https://doi.org/10.1038/s41550-021-01451-8)

Strassmeier, K. G., Ilyin, I., & Steffen, M. 2018, *A&A*, 612, A44, doi: [10.1051/0004-6361/201731631](https://doi.org/10.1051/0004-6361/201731631)

Strassmeier, K. G., Ilyin, I., Järvinen, A., et al. 2015, *Astronomische Nachrichten*, 336, 324, doi: [10.1002/asna.201512172](https://doi.org/10.1002/asna.201512172)

STScI. 2011, Kepler/KIC, STScI/MAST, doi: [10.17909/T9059R](https://doi.org/10.17909/T9059R)

—. 2016, Kepler/EPIC, STScI/MAST, doi: [10.17909/T93W28](https://doi.org/10.17909/T93W28)

Tayar, J., Ceillier, T., García-Hernández, D. A., et al. 2015, *ApJ*, 807, 82, doi: [10.1088/0004-637X/807/1/82](https://doi.org/10.1088/0004-637X/807/1/82)

Teske, J. K., Khanal, S., & Ramírez, I. 2016, *ApJ*, 819, 19, doi: [10.3847/0004-637X/819/1/19](https://doi.org/10.3847/0004-637X/819/1/19)

Wang, E. X., Nordlander, T., Buder, S., et al. 2024, *MNRAS*, 528, 5394, doi: [10.1093/mnras/stae385](https://doi.org/10.1093/mnras/stae385)

Waskom, M. L. 2021, *Journal of Open Source Software*, 6, 3021, doi: [10.21105/joss.03021](https://doi.org/10.21105/joss.03021)

Wenger, M., Ochsenbein, F., Egret, D., et al. 2000, *A&AS*, 143, 9, doi: [10.1051/aas:2000332](https://doi.org/10.1051/aas:2000332)

Wheeler, A. J., Abruzzo, M. W., Casey, A. R., & Ness, M. K. 2023, *AJ*, 165, 68, doi: [10.3847/1538-3881/acaad](https://doi.org/10.3847/1538-3881/acaad)

Wood, M. L., Mann, A. W., & Kraus, A. L. 2021, *AJ*, 162, 128, doi: [10.3847/1538-3881/ac0ae9](https://doi.org/10.3847/1538-3881/ac0ae9)

Xiang, M., & Rix, H.-W. 2022, *Nature*, 603, 599, doi: [10.1038/s41586-022-04496-5](https://doi.org/10.1038/s41586-022-04496-5)

Xiang, M., Ting, Y.-S., Rix, H.-W., et al. 2019, *ApJS*, 245, 34, doi: [10.3847/1538-4365/ab5364](https://doi.org/10.3847/1538-4365/ab5364)

Yong, D., Casagrande, L., Venn, K. A., et al. 2016, *MNRAS*, 459, 487, doi: [10.1093/mnras/stw676](https://doi.org/10.1093/mnras/stw676)

Zahn, J. P. 1977, *A&A*, 57, 383

Zhang, M., Xiang, M., Zhang, H.-W., et al. 2021, *ApJ*, 922, 145, doi: [10.3847/1538-4357/ac22a5](https://doi.org/10.3847/1538-4357/ac22a5)

Zinn, J. C., Stello, D., Elsworth, Y., et al. 2022, *ApJ*, 926, 191, doi: [10.3847/1538-4357/ac2c83](https://doi.org/10.3847/1538-4357/ac2c83)

Zucker, S. 2003, MNRAS, 342, 1291,  
doi: [10.1046/j.1365-8711.2003.06633.x](https://doi.org/10.1046/j.1365-8711.2003.06633.x)